

**UNDER GRANTS IN AID SCHEME OF  
(ER & IPR)  
Project Code**

**PROJECT TITLE:** Self-healing and self-cleaning epoxy thermosetting  
nanocomposites

<b>PI NAME</b>	Dr. Sajal Kumar Das	Chemical Sciences	Tezpur University
<b>CO-PI NAME</b>	Dr. Niranjana Karak	Chemical Sciences	Tezpur University



Project Start Date: 17/12/21  
Project Closure Date: 16/12/24

Year of Completion: 2024  
Department of Chemical Sciences  
TEZPUR UNIVERSITY  
Tezpur – 784028, Assam

## PROJECT TEAM

Sl. No	Name	Designation
1	Dr. Sajal Kumar Das	PI
2	Dr. Niranjana Karak	CO-PI
3	Kriti Yadav	SRF
4	Kriti Yadav	JRF

## DOMAIN SCIENTIST

Sl. No	Name	Designation	Lab
1	Dr. Debdatta Ratna	Scientist G and Head of the Polymer Science & Technology Directorate, NMRL	Naval Materials Research Laboratory
2	Dr. Sangram K Rath	Scientist F	Naval Materials Research Laboratory
3	Sh Rahul Yadav	Scientist B	Naval Materials Research Laboratory

## List of Publications

### Journals

1. K. Yadav, D. Ratna and N. Karak. Gallic acid ester-based flexible UV-shielding epoxy thermosets with tunable properties. **Journal of Macromolecular Science, Part A**, 61(1), 53-68
2. K. Yadav, K. Dutta, R. Poudel and N. Karak. Biocomposites for automotive applications. In *Advances in Biocomposites and their Applications* (pp. 257-284). **Woodhead Publishing**.
3. K. Yadav, D. Ratna, N. Karak, S. Das. Development of Self-Healing and Self-Cleaning Epoxy Thermosets through Diels-Alder Reaction and Functionalized ZnO Nanoparticles. (Manuscript under preparation)

### Conferences

1. K. Yadav and N. Karak. Biobased flexible UV shielding epoxy coatings from gallic acid derivative, SPSI-MACRO 2023, IIT Guwahati.
2. K. Yadav and N. Karak. Tailoring Thermomechanical Properties of UV-Shielding Biodegradable Epoxy Thermosets via Chain Length Modulation. SusChemHeca-2024, Tezpur University.

## Executive Summary

We designed the synthesis of a self-healing and self-cleaning epoxy thermoset to address the inherent brittleness of epoxy resin, which makes it prone to cracks and damages. The self-cleaning property was achieved by incorporating functionalized ZnO nanoparticles.

## Project Objectives

- i) To synthesize hyperbranched epoxy resin from the commercially available reactants including bio-based by the conventional technique.
- ii) To prepare functionalized carbon based nanomaterial by a facile route using easily available raw materials.
- iii) To prepare hyperbranched epoxy /carbon nanohybrid based nanocomposite from the synthesized epoxy and nanomaterial by the conventional technique.
- iv) To characterize the structure and morphology of the prepared epoxy, nanomaterial, and nanocomposites by FTIR, NMR, XRD, XPS, SEM, TEM, etc. studies.
- v) To study the performance characteristics like self-healing and self-cleaning attributes of the characterized epoxy nanocomposites. The physical, mechanical, thermal, chemical, anticorrosion, etc. properties will also be studied.
- vi) To compare the performance characteristics of the nanocomposites with varying composition and processing conditions in order to obtain the best nanocomposite among them.
- vii) To explore the best nanocomposite as a potential self-healing and self-cleaning material for it possible commercialization.

## Project Achievements

1. A self-healing epoxy thermoset was synthesized and characterized based on the Diels-Alder reaction.
2. A self-cleaning epoxy thermoset was prepared and characterized using ZnO nanoparticles.
3. A series of flexible UV-shielding epoxy thermosets with tunable properties were prepared using gallic acid and varying length of PEGs.

## 4 List of Equipment Acquired under Grants in Aid Project

Sl. No.	Name of Equipment/ Software/Accessories	Cost (in lakhs)	Retained by Institute	Purchase Year
	No Equipment Acquired			

# CONTENT

List of Equipment Acquired under Grants in Aid Project .....	iii
CONTENT .....	iv
1. Introduction.....	1
2. Literature Survey .....	1
3. Chapter 1 .....	2
4. Chapter 2 .....	11
5. Chapter 3 .....	16
6. Chapter 4 .....	29
7. Traceability Matrix: Objectives and Work done .....	46
8. Feedback from Lab/ Domain Scientist .....	47
9. Traceability Matrix: Milestone Reports and Work done .....	47
10. Traceability Matrix: Publications and Work done .....	48
11. Future Work: Extensions and Exploitation.....	48
<i>References</i> .....	48

Sl. No.	Name	Institute Name	JRF/ SRF/ RA/PA	Time (Worked on project)
1.	Kriti Yadav	Tezpur University	JRF, SRF	2 years 6 months

## List of Figures

Figure 1: Reaction scheme for formation of gallic acid ester and its epoxy resin

Figure 2: PXRD pattern of thermosets

Figure 3: FTIR spectra of Gallic acid (GA), Gallic acid ester (ES), Epoxy of gallic acid ester (EP) and its thermoset (EH)

Figure 4: <sup>1</sup>H NMR spectrum of ES

Figure 5: <sup>13</sup>C NMR spectrum of ES

Figure 6: <sup>1</sup>H NMR spectrum of EP

Figure 7: <sup>13</sup>C NMR spectrum of EP

Figure 8: Stress versus strain curves of epoxy thermosets



Figure 9: (a) TGA thermograms (b) DTG curves indicating three stage degradation, and (c) DSC curves displaying glass transition temperatures for the prepared epoxy thermosets

Figure 10: UV transparency curve of the prepared thermoset

Figure 11: Reaction scheme for synthesis of glycolic acid and 4,4'-Oxydianiline-based epoxy

Figure 12: Reaction scheme for synthesis of 2,2' Bis(hydroxymethyl)propionic acid and 4,4'-Oxydianiline-based epoxy

Scheme 3: Synthesis of vanillin- cystamine based epoxy

Scheme 4: Synthesis of Vanillin-hexamethylenediamine based epoxy

Figure 13: Reaction scheme for the synthesis of PEG-4,4'-(4,4'-Isopropylidenediphenyl-1,1'-diylldioxy)dianiline-IPDI based curing agent

Figure 14: Reaction scheme for the synthesis of PEG-Melamine-IPDI-based curing agent

Figure 15: Reaction scheme for the synthesis of PEG-Hexamethylenediamine-IPDI based curing agent

Figure 16: <sup>1</sup>H NMR spectra of (a)Cystamine (b) cystamine based epoxy, <sup>13</sup>C NMR spectra of (c)cystamine (d)cystamine based epoxy

Figure 16: FTIR spectra of vanillin, vanillin-based imine, and its epoxy (VCIE)

Figure 17: Stress-strain curve of epoxy cured with PAA

Figure 19: Plausible reaction scheme for the formation of gallic acid ester and its epoxy resin

Figure 20: Crosslinking of EP with PAA to obtain the thermoset (ET)

Figure 21: (a) FTIR spectra of Gallic acid (GA), Gallic acid ester (ES), Epoxy of gallic acid ester (EP) and its thermoset (EH), (b) All the epoxy resins prepared using esters of varying chain lengths, and (c) Enlarged spectra of epoxy resin and corresponding thermoset depicting curing process

Figure 22: <sup>1</sup>H NMR spectrum of (a) ES 2, (c) EP 2 and <sup>13</sup>C NMR spectrum of (b) ES 2, (d) EP 2

Figure 23: (a) Stress-strain curves and (b)PXR pattern of cured epoxy thermosets

Figure 24: (a) Shear stress and (b) viscosity of the epoxy resins as a function of shear rate

Figure 25:(a) XPS survey spectra of the epoxy thermoset ET 2 and their high-resolution deconvoluted spectra of (b) C 1s, (c) N 1s, and (d) O 1s peaks.

Figure 26: (a) TGA thermograms (b) DTG curves indicating three-stage degradation, and (c) DSC curves displaying glass transition temperatures for the prepared epoxy thermosets

Figure 27: (a) UV transparency curve of the prepared thermoset in the UV-vis range and (b) digital photographs of the thermosets

Figure 28: Optical density curves of (a) BS strain and (b) PA strain measured against time for a duration of 25 days (c) Weight loss (%) profiles, SEM images of the thermosets (d) before and after degradation test using (e) BS and (f) PA strain.

*Scheme 4: Plausible reaction scheme for the formation of furfuryl alcohol-based epoxy resin and the corresponding thermoset*

Figure 29: Digital images of the cured thermosets

Figure 30: (a) FTIR spectra of FGE, FGE-CYS, BMI, and FGE-CYS-BMI, (b) spectra showing comparison between the pristine thermoset FGE-CYS-BMI-80, thermoset cured at 130°C (FGE-CYS-BMI-130) and post cured at 80°C (FGE-CYS-BMI-80)

Figure 31:  $^1\text{H}$  NMR spectrum of (a) CYS and (b)  $^{13}\text{C}$  NMR spectrum of CYS

Figure 32:  $^1\text{H}$  NMR spectrum of FGE

Figure 33:  $^{13}\text{C}$  NMR spectrum of FGE

Figure 34:  $^1\text{H}$  NMR spectrum of FGE-CYS

Figure 35:  $^{13}\text{C}$  NMR spectrum of FGE-CYS

Figure 36: DSC curves displaying glass transition temperatures for the prepared epoxy thermosets

Figure 37: PXRD pattern of epoxy thermosets

Figure 38: Stress-strain curve of pristine epoxy thermosets

Figure 39: Stress-strain profiles of pristine along with their respective healed thermosets

Figure 40: Photographs of the cut and healed thermosets (a) FGE-CYS-BMI (1:1.5), (b) FGE-CYS-BMI (1:1), (c) FGE-CYS-BMI (1:0.5), (d) FGE-CYS-BMI (1:0.33)

Figure 41: UV-visible absorption spectra of ZnO nanoparticles

Figure 42: FTIR spectra of (a) ZnO NPs, (b) Spectra of ZnO NPs along with the nanocomposite, and the pristine thermoset

Figure 43: PXRD pattern of synthesized ZnO NPs

Figure 44: SEM images of ZnO particles showing their morphology at three different resolutions

Figure 45: CA measurements of (a) FGE-CYS-BMI(1:1), (b) FGE-CYS-BMI-Z(5%) and (c) FGE-CYS-BMI-Z(10%)

Figure 46: Self-cleaning test of (a) FGE-CYS-BMI(1:1), (b) FGE-CYS-BMI-Z(5%) and (c) FGE-CYS-BMI-Z(10%)

### **List of Tables**

Table 1: Physical characteristics of the prepared epoxy thermosets

Table 2: Chemical resistance studies for 30 days of the epoxy thermoset prepared using different amount of hardener

Table 3: Mechanical properties of the epoxy resins along with their cured thermosets

Table 4: Chemical resistance studies for 30 days of the epoxy thermosets

Table 5: Weight loss ( $T_{wt\%}$ ) of the cured thermosets along with their percent char residue at 600°C

Table 6: Optimization of curing time and curing temperature

Table 7: Glass transition temperature of the thermosets

Table 8: Mechanical properties of the epoxy resins along with their thermosets

Table 9: Mechanical properties of the pristine along with their healed thermoset

## 1. Introduction

Epoxy resins containing multiple epoxide rings are transformed into thermosetting polymers and widely utilized across various industries, including aerospace, automotive, marine, packaging, coatings, electronics, composites, and adhesives. Their outstanding properties make them a preferred choice in these sectors [1,2]. In fact, the global market value of epoxy resins as adhesives was valued at USD 6.8 billion in 2020, with expectations for a 5.6% compound annual growth rate in a couple of years, indicating the high demand for epoxy thermosets in applications such as adhesives, coatings, paints, and composite matrices [3].

Traditionally, commercially available epoxy resins are predominantly derived from bisphenol-A (BPA), which is synthesized from phenol, a petroleum-based product [4]. However, BPA has raised concerns due to its adverse effects on human health. It has been identified as a metabolic disruptor and a potential antagonist to androgen receptors, as well as a disruptor of estrogen hormones [5]. The primary exposure to BPA occurs when it leaches from polymeric materials into food products, leading to ingestion [6]. Consequently, material scientists have increasingly focused on finding bio-based alternatives to BPA, aiming to create epoxy thermosets with similar desirable properties. Given its structural resemblance to BPA, naturally occurring phenolic or polyol compounds have emerged as promising raw materials for the synthesis of bio-based epoxy resins [7]. Several renewable resources, including natural oils [8], cardanol [9], lignin [10], itaconic acid [11], isosorbide [12], wood [13], tannic acid [14], lactic acid [15], and sugars [17], have been explored in recent years for this purpose. In this investigation, gallic acid has been selected as the bio-based material for synthesizing epoxy resin.

Metals, on the other hand, face corrosion when exposed to air and moisture, leading to oxidation and reduced service life, which poses significant economic challenges globally [17]. A common and cost-effective method to protect metals is by applying organic coatings, which act as a physical barrier to moisture and other corrosive agents, thus delaying the onset of corrosion. However, traditional coatings, especially those based on epoxy resins, often fail to provide long-term corrosion protection [18]. These coatings can be permeable to oxygen and aggressive ions, and their inherent brittleness may lead to micro-cracks over time, compromising the mechanical properties of the material [19]. To overcome these limitations and enhance the longevity and reliability of the material, the integration of self-healing properties into smart coatings has gained attention. This can be achieved through the incorporation of reversible physical and chemical interactions, such as dynamic covalent bonds, which allow the material to autonomously repair itself upon crack formation. Examples of dynamic bonds used for self-healing include disulfide bonds [20], boronic ester bonds [21], and urea bonds [22]. Noncovalent interactions like hydrogen bonds, ionic interactions, and metal-ligand coordination can also be employed [23]. The healing process can be triggered by various external stimuli, such as heat, sunlight, microwave or infrared radiation, electric or magnetic fields, which induce chain mobility, leading to the repair of minor cracks.

## 2. Literature Survey

Canadell et al. in the year 2011, a cross-linked pre-polymer resin containing disulfide groups with tetrafunctional thiols, at 60 °C in the presence of 4-(dimethylamino) pyridine. The dynamic disulfide group incorporation provided the polymeric material with a self-healing attribute. It was found that this method is widely applicable in low- $T_g$  materials such as polyurethanes and polyesters. The partial mobility of chains in glassy polymers restricts its applicability to high  $T_g$  materials [25].

Chowdhury et al. in the year 2014, synthesized urea-formaldehyde microcapsules and encapsulated them within the epoxy resin. Impact tests with 30 J and 45 J impact loads created micro-cracks in the composite materials. After the impact test, the impaired area got healed due to the formation of new interactions at the location of the microcrack as a result of bleeding from the microcapsules, and mechanical properties were reinstated by the process of self-healing [26].

Hia et al. in the year 2018, synthesized two self-healing systems, the dual-capsule self-healing system and the capsule-catalyst self-healing system. In the dual-capsule self-healing system, both the microcapsules that are alginate/epoxy and alginate/mercaptan microcapsules were incorporated into the epoxy matrix, whereas alginate/epoxy microcapsule and  $\text{Sc}(\text{OTf})_3$  catalyst were used for the capsule-catalyst system. The dual-capsule self-healing system exhibited a greater number of healing cycles as compared to the capsule-catalyst self-healing system [27].

Zhang et al. in the year 2021 synthesized a biobased epoxy resin through a thermally induced thiol-epoxy click reaction between dithiol-functionalized boronic ester and epoxidized vegetable oils. The prepared epoxy thermoset showed high tensile strength, excellent self-healing, elongation at break, and reprocessable properties due to the synergistic incorporation of three dynamic covalent units such as S-S bonds, carboxylic ester units, and boronic ester units [28].

### **3. Chapter 1: Synthesis of a flexible bio-based epoxy resins based on gallic acid and PEG-200.**

**3.1. Purpose:** Synthesis of a bio-based epoxy resins and its study of the variation in properties with varying amount of cross-linker.

**3.2. Details of protocol/Workdone:**

Gallic acid (molecular weight  $170.12 \text{ g mol}^{-1}$ ), poly(ethylene glycol) ( $M_n$  200 g/mol) (PEG 200) and para-Toluene sulphonic acid (pTSA) were procured from Sisco Research Laboratories Pvt. Ltd., India. Epichlorohydrin, sodium chloride (NaCl), sodium hydroxide (NaOH), and anhydrous sodium sulfate ( $\text{Na}_2\text{SO}_4$ ) were procured from Merck, India. Poly(amido amine) which was used as a hardener was offered by Asian Paints, India. Tetrahydrofuran (THF) and acetone were procured from S.D. Fine Chem Ltd, India and were used post distillation.

#### **Preparation of Gallic acid ester**

Gallic acid ester was prepared by condensation of PEG 200 (1.4 mL, 0.0079 mol) with gallic acid (2.7 g, 0.0159 mol) along with catalytic amount of pTSA. All these reactants were taken together in a three neck round bottom flask and the condensation reaction was carried out at 160 °C for 2 h, the condensation process was carried forward with the help of a vacuum suction

pump to draw water molecules from the reaction vessel that were released in the course of the reaction.

### Preparation of Gallic acid ester-based epoxy resin

The Gallic acid ester-based epoxy resin was prepared by the usual epoxide formation approach involving polycondensation reaction between gallic acid ester polyol and epichlorohydrin at 70 °C for 2 h with aqueous NaOH added dropwise and being used as the base. Gallic acid ester (4.47 g, 0.0088 mol) and epichlorohydrin (12.5 mL, 0.159 mol) were taken in a 100 mL three necked round-bottomed flask equipped with a dropping funnel, a mechanical stirrer, a thermometer, and an oil bath. A 5 N aqueous solution of NaOH (2.13 g, 0.0088 mol) was introduced to this reaction mixture dropwise using a pressure-equalizing funnel (2–2.5 h). After complete addition of NaOH, the reaction was carried on for additional 2 h at 70 °C. The reaction mixture was then left undisturbed to settle in a separating funnel, followed by removal of the aqueous layer from the desired organic layer. The organic layer was washed with 16% brine solution followed by fresh water 2–3 times to eliminate water-soluble impurities along with the unreacted reactants. Finally, the epoxy resin was obtained by drying the organic layer at 70 °C (after solubilizing in THF) under vacuum with the help of a rotary evaporator to remove spare epichlorohydrin and entrapped water from the resin. The end product obtained was a sticky viscous transparent light-brown mass coded as EP. The complete synthetic route is shown in Figure 1(Scheme 1).

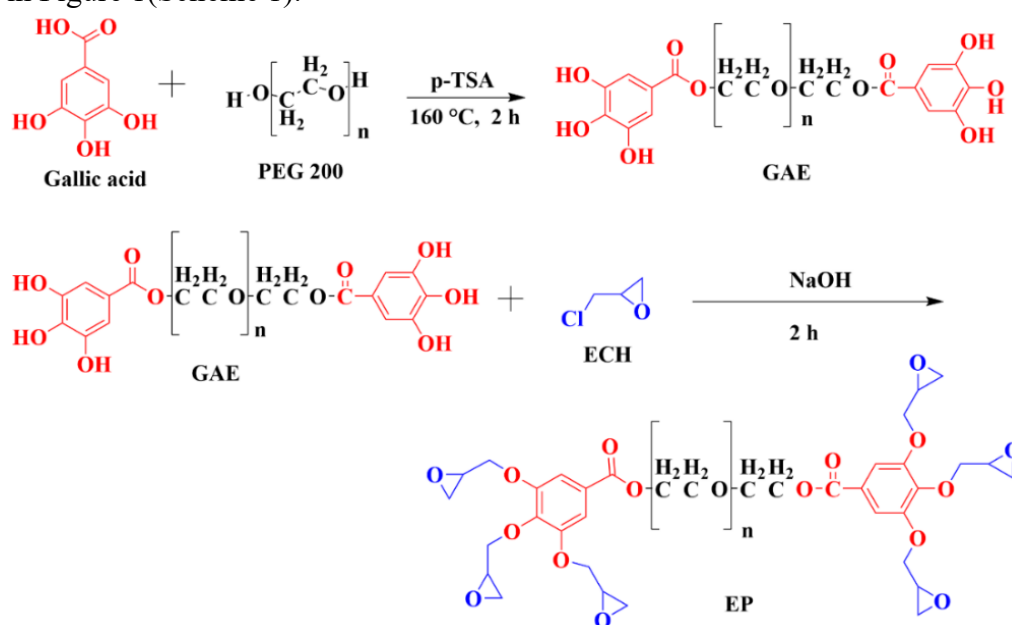


Figure 1: Reaction scheme for formation of gallic acid ester and its epoxy resin

### Curing of resin

The prepolymer epoxy resin was converted to a three-dimensional network polymer by curing them with biobased poly(amido amine) hardener. So, a uniform mixture of resin was prepared with 40 phr (parts per hundred grams of resin) and 50 phr of the hardener. The mixture was taken in a 25 mL beaker and mixed by hand stirring using minimum volume of THF as the solvent at room temperature to obtain a homogeneous mixture coded as EP40 and EP50, respectively. The mixtures were degassed to remove excess solvent in a vacuum desiccator which were then uniformly spread on tin plates and glass plates for impact resistance, gloss,

and chemical resistance tests. The epoxy coated plates after becoming touch-free were cured at a temperature of 100 °C for 1h followed by its post curing at 120 °C for 20 mins. The curing and post curing time were optimized by examining the swelling value of the prepared films in THF, which lies between 20 and 30%.

### **Instrumentation and Methods:**

FTIR spectrum of the synthesized epoxy resin was recorded using Nicolet FTIR spectrophotometer (Impact-410, USA) employing KBr pellets within 4000–500  $\text{cm}^{-1}$ . NMR study was done on a Bruker Biospin AG 500 MHz NMR spectrometer (Model- Avance III HDX, USA) using  $d_{kk}$ -DMSO,  $\text{CDCl}_3$  as the solvent and tetramethylsilane (TMS) as the internal standard.

Mechanical properties like tensile strength, toughness and elongation at break were recorded with the help of Universal Testing Machine (UTM, model- WDW-10, Jinan, China) with a 0.5 kN load cell. Scratch hardness test of unpeeled thermosets films cast on glass slides was carried out by using Scratch hardness tester (Sheen instrument Pvt. Ltd., U.K) and impact resistance by Impact tester (S.C. Dey Co., Kolkata) as per the standard falling ball method. The gloss characteristics of the cured films were found out by using mini glossmeter (Sheen instrument Ltd, U.K), over resin coated mild steel plate at an angle of incidence of 60°. Thermal stability of the prepared epoxy films was analysed using TGA 4000 (PerkinElmer) thermal instrument, under nitrogen atmosphere (flow rate of 30  $\text{mL min}^{-1}$ ), in the temperature range of 32–720 °C (heating rate: 10 °C  $\text{min}^{-1}$ ). Chemical resistance of the cured films was performed in different chemical environments. The cured thermosets were kept in glass vials in various chemical media such as 5% aqueous solutions of HCl, 5% aqueous solutions of NaOH, 10% aqueous solutions of NaCl, 10% aqueous solutions of EtOH and tap water at room temperature for 15 days and examined for change in weight and physical characteristics of the films. Transparency of the epoxy thermosets was assessed by measuring the transmittance percentage of 25 mm × 10 mm × 0.3 mm thermosets with the help of Evolution-300 UV–visible spectrophotometer (Thermo Fischer, USA) in the range of wavelength 200–800 nm.

To determine the flow properties of the synthesized resins, viscosity measurement was done using a rotational rheometer (Anton Paar, Austria, Model: MCR 72) equipped with stainless steel parallel plate of diameter 25 mm. The sheer rate was swept from 1–1000 1/s under a steady state flow with a gap of 1 mm.

A bacterial biodegradability test was carried out following the McFarland turbidity method gram-using *Pseudomonas aeruginosa* (PA) and *Bacillus subtilis* (BS). The bacterial strains were cultured in different culture mediums which were used after sterilization and incubation. 100  $\mu\text{L}$  aliquot of the cultured bacterial medium was added to a conical flask containing 10 mL of the sterilized broth solution. Sterilized thermosets were placed in the conical flask containing the cultured bacterial medium followed by incubation at 37 °C. The rate of bacterial degradation of the thermoset was determined by measuring the optical density of the culture medium using a UV-vis spectrophotometer at a wavelength of 600 nm for a period of 30 days. The weight loss profile of the thermosets was calculated after the test and their surface morphologies were studied using Scanning Electron Microscope (SEM).

### 3.3: Results and discussion:

**Structural analysis:** The physico-chemical structure of the synthesized epoxy was analysed to authenticate its proposed structure.

#### XRD study

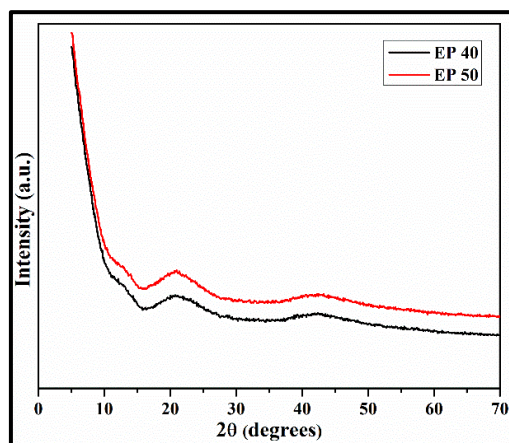


Figure 2: PXRD pattern of thermosets

X-ray diffractograms of the thermosets are shown in Figure 2, which reveal the absence of any sharp peak indicating amorphous nature of the thermosets.

#### FTIR study

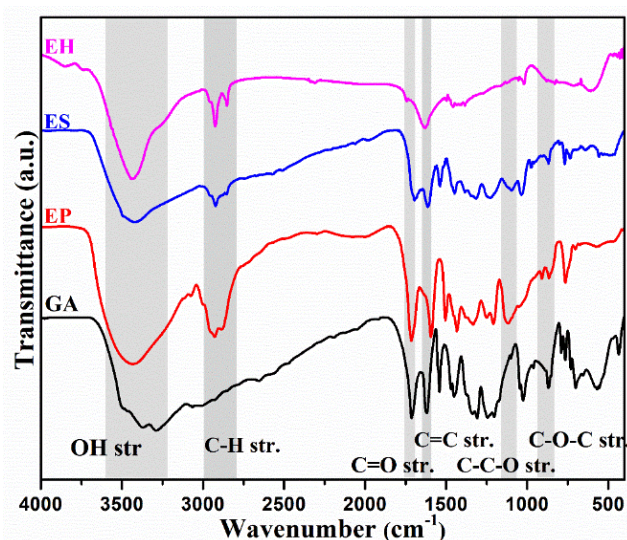


Figure 3: FTIR spectra of Gallic acid (GA), Gallic acid ester (ES), Epoxy of gallic acid ester (EP) and its thermoset (EH)

In the FTIR spectra (Figure 3) characteristic absorption band at around  $3434\text{ cm}^{-1}$  (OH stretching),  $1610\text{ cm}^{-1}$  (C=C aromatic ring) appears in all the four spectra. Characteristic absorption peaks at  $1696\text{ cm}^{-1}$  (C=O stretching),  $1234\text{ cm}^{-1}$  (C-C-O stretching at carbonyl C),  $1095\text{ cm}^{-1}$  (O-C-C stretching of the alkyl part of ester),  $2925\text{ cm}^{-1}$  and  $2869\text{ cm}^{-1}$  ( $\text{CH}_2$  asymmetric and symmetric stretching vibrations) in the spectra of ES might be indicative of esterification taking place. Appearance of characteristic absorption peaks at  $868\text{ cm}^{-1}$  and  $912\text{ cm}^{-1}$  in the spectra of EP which can be attributed to asymmetric stretching and C-O-C stretching



of oxirane ring, respectively which was initially absent in the ester (ES) supporting successful epoxide formation of the gallic acid ester moiety. These peaks were absent in the spectrum of EH thermoset which occurs due to crosslinking of the resin with the hardener resulting in opening of the epoxy.

### NMR spectral analysis

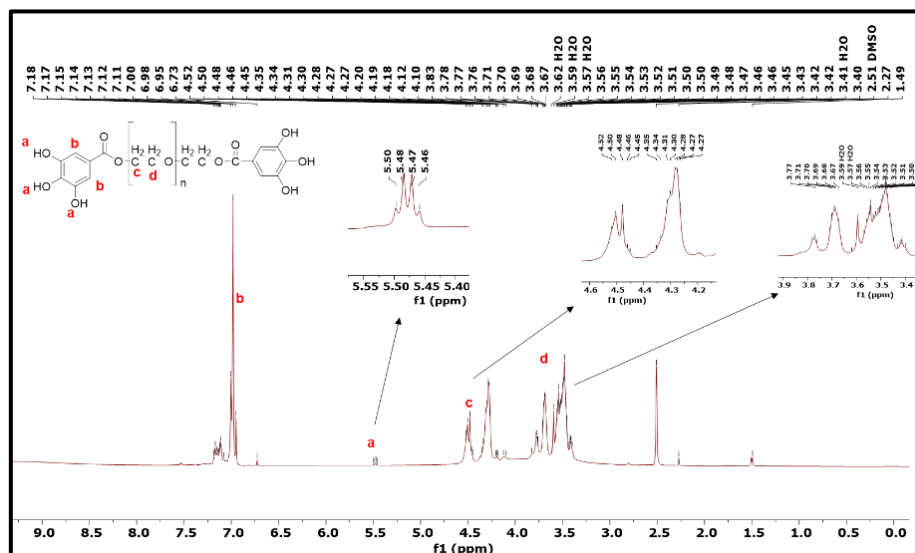


Figure 4:  $^1\text{H}$  NMR spectrum of ES

The  $^1\text{H}$  NMR (DMSO) spectrum of ES is shown in the Figure 4. Peak at  $\delta=7$  ppm is due to protons directly attached to phenyl ring of gallic acid moiety in the molecule. Small peak at  $\delta=5.47$  is due to hydroxyl proton and its lower intensity might be due to H-bonding between two different synthesized ester moieties. Due to change in stereochemistry the  $\text{CH}_2$  protons near ester group showed a double doublet at  $\delta=4.4$  ppm and  $\text{CH}_2$  protons attached next to ester group also show a double doublet at 3.75 ppm. The other peaks of lower intensity might be due to unused catalyst pTSA and other impurities.

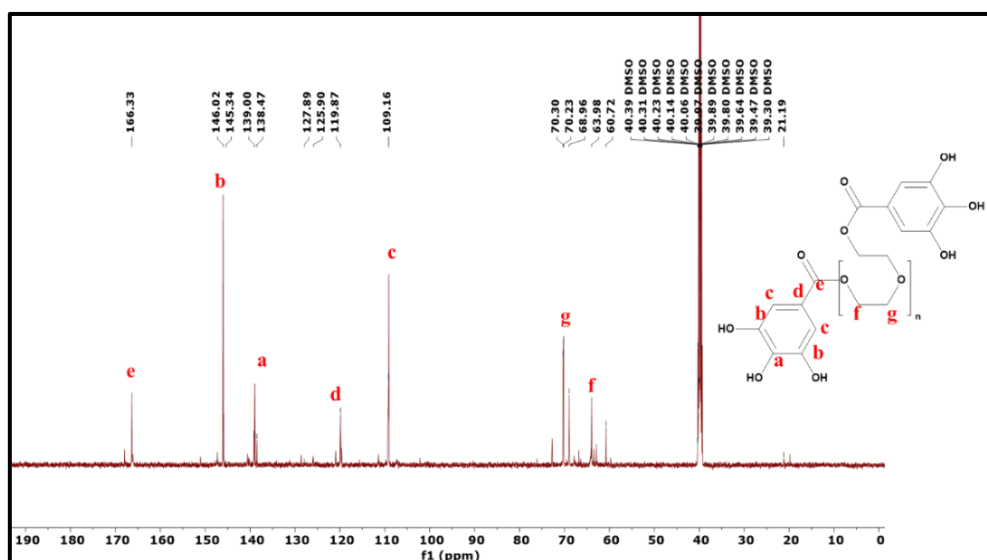
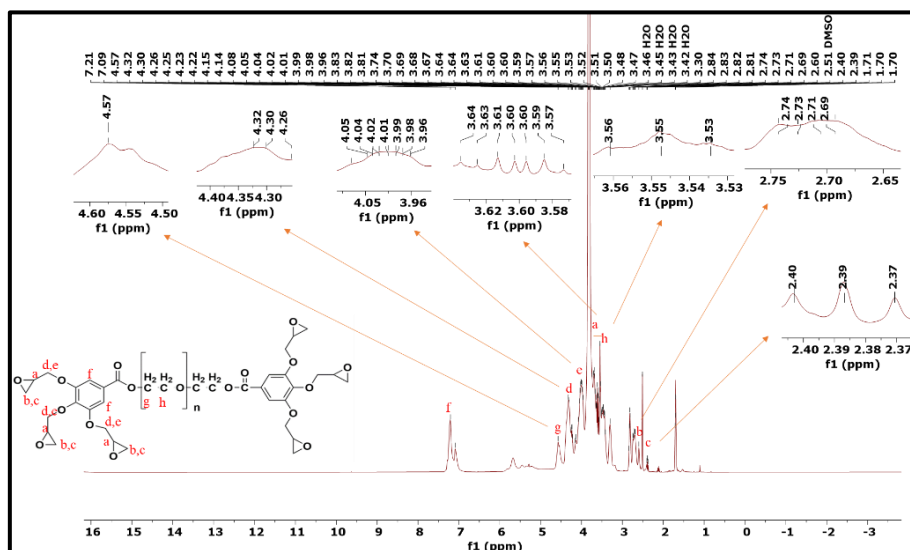


Figure 5:  $^{13}\text{C}$  NMR spectrum of ES

The  $^{13}\text{C}$  NMR (DMSO) spectrum is shown in Figure 5. Peak at  $\delta=166.3$  ppm is due to carbonyl C. Peak at  $\delta=146.02$  ppm is due to C attached to hydroxyl group near the carbonyl C. Peak at  $\delta=139$  ppm is due to the C attached to hydroxyl group farther from the carbonyl C. Peaks at  $\delta=119.87$ , and  $109.16$  ppm are due to aromatic Cs. Peaks at  $\delta=70.23$  and  $63.98$  ppm are due to Cs on the alkyl chain of PEG moiety. The other peaks of lower intensity might be due to unused catalyst pTSA and other impurities.



The  $^{13}\text{C}$  NMR (DMSO) spectrum of EP is shown in Figure 7. Peak at  $\delta=165.66$  ppm is due to the carbonyl C. Peak at  $\delta=152.15$  ppm is due to the aromatic Cs attached to O linked to the chain bearing the oxirane ring which is close to the ester linkage. Peak at  $\delta=141.97$  ppm is due to the aromatic C attached to O linked to the chain bearing the oxirane ring which is farther from ester linkage. Peak at  $\delta=125.17$  ppm is due to the aromatic C next to the carbonyl group. Peak at  $\delta=112.15$  ppm is due to the unsubstituted aromatic Cs. Peak at  $\delta=152.15$  ppm is due to the aromatic Cs attached to O linked to the chain bearing the oxirane ring. Peaks at  $\delta=70.12$ , and  $67.46$  ppm are due to the Cs next to the oxirane ring. Peaks at  $\delta=69.07$ , and  $60.14$  ppm are due to the alkyl Cs of the PEG moiety. Peaks at  $\delta=50.15$ , and  $44.08$  ppm are due to the Cs of the oxirane ring. The other peaks of lower intensity might be due to opening of oxirane ring and other impurities.

### Physical and mechanical properties

The physical properties including color, transparency, gloss, specific gravity, etc. of the epoxy thermosets were determined and tabulated in Table 1. Stress-strain curve with toughness of the thermosets prepared using different amount of hardener are shown in Figure 8. These physical properties are comparable with other commercially available epoxy thermosets and hence acceptable for their utilization in different applications. The mechanical properties like tensile strength, elongation at break, toughness, impact resistance, scratch hardness, etc. of the epoxy thermosets are given in Table 1. From the results, it was found that EP50 thermoset exhibited higher mechanical properties including tensile strength, elongation, toughness and impact resistance values than EP40. This is due to the fact that EP50 possessed higher crosslinking and more plasticization effect because of the presence of higher amount of poly (amido amine) hardener. This resulted higher numbers of chain crosslinking but at the same time as the hardener possessing plasticization effect because of long chain fatty acid moieties, so both tensile strength and elongation values are higher for EP50 than EP40 thermoset. Thus, the toughness, which is the product tensile strength and elongation at break, was also higher for the former than the later. The overall high mechanical performance of both the thermosets is because of the proper combination of aliphatic and aromatic moieties in the branched structural architecture.

**Table 10: Physical characteristics of the prepared epoxy thermosets**

Sample Code	EP 40	EP 50
Color	Light brown	Light brown
Tensile strength (MPa)	5.4	8.9
Elongation at break (%)	90.58	146.27
Toughness ( $\text{J/m}^3$ )	406.5	1087
Impact resistance ( $\text{kJ/m}^2$ )	>19.3	>19.3
Gloss ( $60^\circ$ )	81.04	84.5
Scratch resistance (kg)	3	2.5
Specific gravity of resin	2.39	

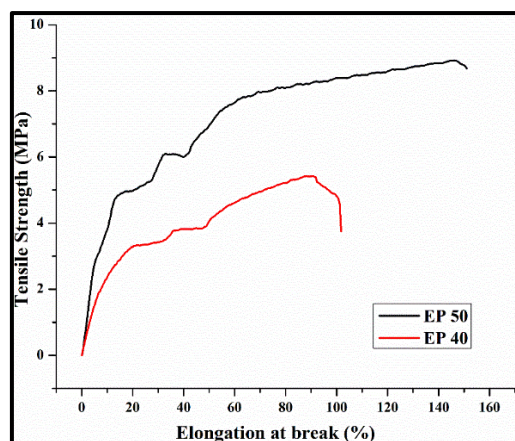


Figure 8: Stress versus strain curves of epoxy thermosets

### Chemical resistance studies

The pristine polymer does not show excellent chemical resistance which may be due to the hydrolysable ester group present in the structure of thermosets.

Table 11: Chemical resistance studies for 30 days of the epoxy thermoset prepared using different amount of hardener

Types of media	Weight Changes (%)	
	EP 40	EP 50
Alkali (0.5%)	4.6	4.9
NaCl (10%)	2.7	1.6
HCl (10%)	3.9	3.5
Tap Water	0.50	0.32
Ethanol (20%)	0.69	0.88

### Thermal properties of the epoxy thermosets

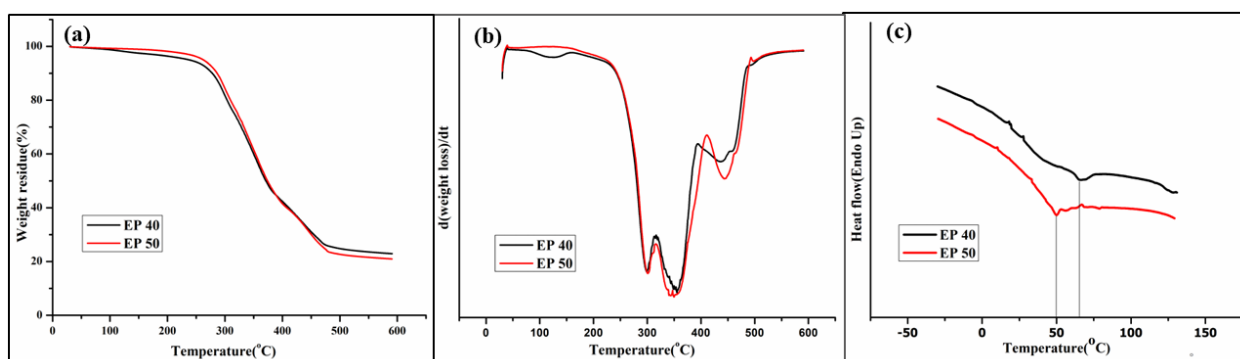


Figure 9: (a) TGA thermograms (b) DTG curves indicating three stage degradation, and (c) DSC curves displaying glass transition temperatures for the prepared epoxy thermosets

Thermostability of epoxy thermoset is an important property as it extends end-use of the material across a broad range of temperature. The thermogravimetric analysis was carried out

within the temperature range of 30–600 °C and the TGA thermograms are shown in Figure 9(a). The thermosets exhibited three-stage degradation, the initial 4–5% degradation attributed to the loss of small molecules such as water, THF, and other volatiles entrapped inside the polymeric network. The real degradation started ahead of temperature 240°C. The first stage degradation ranging from 246 °C to 304 °C, might correlate to cleavage of ester bonds and other less thermostable bonds. The next stage of degradation having a  $T_{\text{onset}}$  at around 320 °C and ranging from 320 °C to 372 °C might be due to decomposition of cyclic and other relatively more thermostable moieties and amide linkage in poly (amido amine) which was used as the curing agent. The third stage degradation with a  $T_{\text{onset}}$  at around 420 °C and ranging from 420 °C to 462 °C might be due to decomposition of aromatic rings of GA. The TGA thermogram displays weight residue value of 22.94% and 21.28% for EP40 and EP50, respectively concluding better thermostability of thermoset with more amount of hardener which might be due to greater crosslinking density.

The DSC thermograms as depicted in Figure 9(c) indicates the glass transition temperature of the prepared epoxy thermosets. In this study, EP 40 with 40% of hardener was found to have a  $T_g$  at 65.29°C, whereas EP 50 with 50% of hardener was found to have a  $T_g$  at 50.22 °C. So, increasing the amount of hardener might lead to denser network and reduced the flowability thus increasing the  $T_g$ , but as this hardener has long chain flexible hydrocarbon chain, which has plasticization effect, so overall the  $T_g$  value decreased.

### UV-Transparency of epoxy thermosets

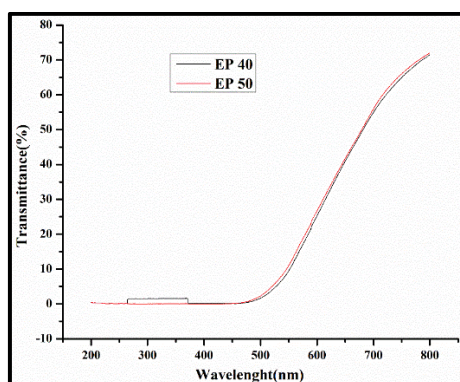


Figure 10: UV transparency curve of the prepared thermoset

Transparency of any material is its potential to transmit visible light across it. Higher the transmittance value, higher is its transparency as more amount of visible light can pass across the polymeric film. Transmittance values for the epoxy thermosets prepared using different amount of hardener were recorded across a wavelength range of 200–800 nm. The prepared epoxy thermosets showed excellent transmittance of about 71% allowing its application in various optical devices as well as in packaging materials. The transmittance percentage of the epoxy thermoset with lesser amount of hardener was slightly lower than the one with greater amount of hardener.

**3.4: Conclusion:** A bio-based epoxy resin was prepared and crosslinked using varying amounts of crosslinker to obtain the optimal thermoset.

## 4. Chapter 2: Synthesis of epoxy resins from bio-based sources (vanillin and cystamine) and non-bio-based sources, along with the development of various curing agents

**4.1. Purpose:** To synthesize a series of epoxy resins and cross-linking agents from bio-based and non bio-based sources.

### 4.2. Details of protocol/workdone:

Vanillin (molecular weight 152.15 g mol<sup>-1</sup>), Cystamine dihydrochloride (M<sub>n</sub> 225.19 g/mol), poly(ethylene glycol) (M<sub>n</sub> 200 g/mol) (PEG 200) and para-Toluene sulphonic acid (pTSA) were procured from Sisco Research Laboratories Pvt. Ltd., India. Glycolic acid, Hexamethylenediamine, Isophorone diisocyanate (IPDI), 4,4'-(4,4'-Isopropylidenediphenyl-1,1'-diylldioxy) dianiline and 4,4'-Oxydianiline were obtained from Sigma Aldrich. Epichlorohydrin, sodium chloride (NaCl), sodium hydroxide (NaOH), and anhydrous sodium sulfate (Na<sub>2</sub>SO<sub>4</sub>) were procured from Merck, India. Poly(amido amine) was offered by Asian Paints, India. Tetrahydrofuran (THF) and acetone were procured from S.D. Fine Chem Ltd, India and were used post distillation.

**Instrumentation and Methods:** As described in details of protocol of Chapter 1.

### Synthesis of Epoxy Resins:

1. **Synthesis of glycolic acid and 4,4'-Oxydianiline-based epoxy:** Glycolic acid (30 mmol) was placed in a two-necked round-bottom flask, and THF with a small amount of DMF was added under an N<sub>2</sub> atmosphere, equipped with a condenser. 4,4'-Oxydianiline (15 mmol) was added dropwise, and the mixture was heated for 1 hour at 75°C and 2.5 hours at 140°C. After the reaction, the solvent was removed using a rotary evaporator to yield a viscous liquid.

For epoxy resin synthesis, 10 mmol of the amide was placed in a two-necked round-bottom flask with a mechanical stirrer. 60 mmol Epichlorohydrin (3 times the hydroxy equivalent weight of the amide) was added and a solution of 10 mmol 0.5 N NaOH solution was added dropwise through a pressure-equalizing funnel at 70°C, maintaining a pH of 7.4. The mixture was further heated for 1–1.5 hours at 80°C with continuous stirring. After cooling to room temperature, the mixture was transferred to a separating funnel, and the aqueous and organic layers were separated. The organic layer was washed with brine and distilled water to remove impurities, then dissolved in THF. Finally, THF and any remaining water were removed via rotary evaporation, yielding the desired viscous epoxy resin. The synthetic scheme is represented below:

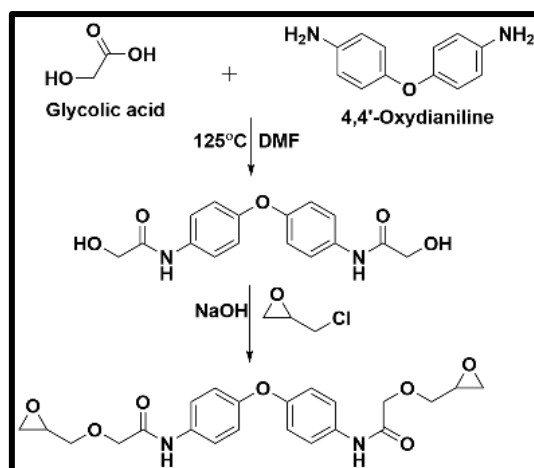


Figure 11: Reaction scheme for synthesis of glycolic acid and 4,4'-Oxydianiline-based epoxy

2. **Synthesis of 2,2' Bis(hydroxymethyl)propionic acid and 4,4'-Oxydianiline-based epoxy:** Similar procedure of amidation reaction was followed as described in the previous scheme followed by epoxidation to obtain the desired amide based epoxy resin.

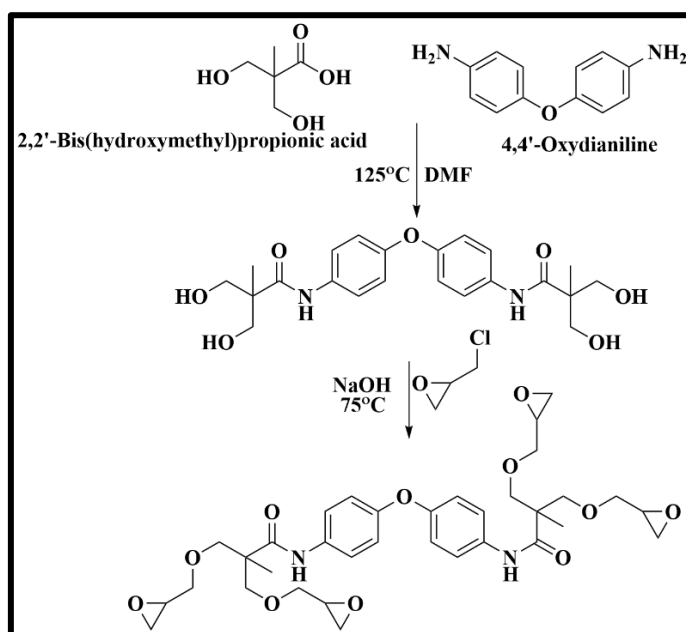
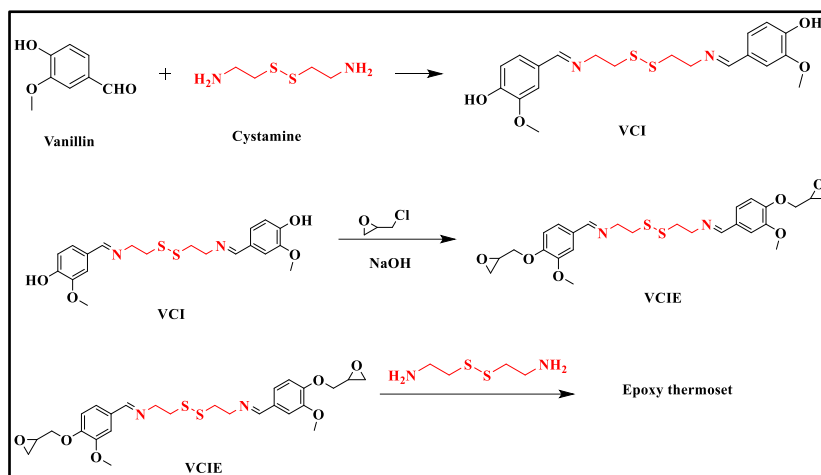
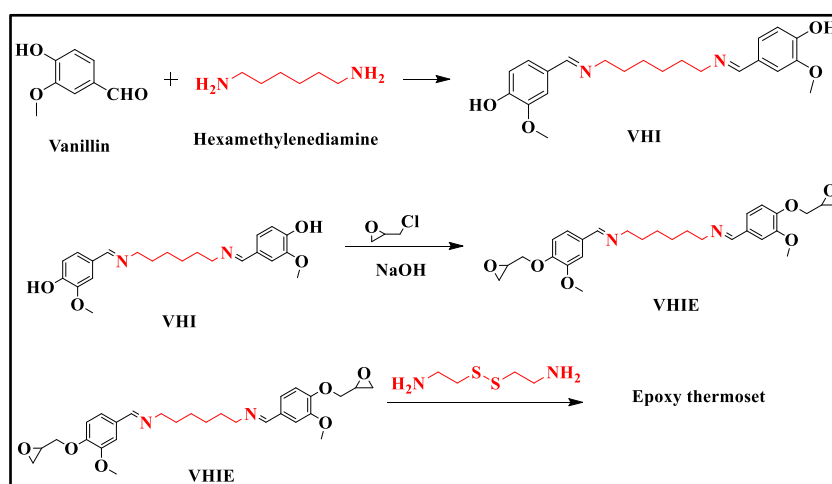


Figure 12: Reaction scheme for synthesis of 2,2' Bis(hydroxymethyl)propionic acid and 4,4'-Oxydianiline-based epoxy

3. **Synthesis of Vanillin based epoxy resin:** The synthetic procedure involves an imidation reaction of Vanillin with diamine (i.e. cystamine (obtained by desalination of cystamine dihydrochloride) and hexamethylenediamine). Here 10 mmol of Vanillin was weighed in a two-necked round-bottom flask which dissolved in DMF to which 5 mmol of cystamine was added and the reaction mixture was stirred vigorously for 1 hour resulting in the desired imine. The crude vanillin-based imine was epoxidised, as per the general epoxidation procedure gave the desired vanillin-based epoxy.



**Scheme 3: Synthesis of vanillin-cystamine based epoxy**



**Scheme 4: Synthesis of Vanillin-hexamethylenediamine based epoxy**

**Synthesis of curing agents:** Poly(urethane-urea) based curing agents were synthesized using various available substrates.

### 1. Synthesis of PEG-4,4'-(4,4'-Isopropylidenediphenyl-1,1'-diylldioxy)dianiline-IPDI based curing agent

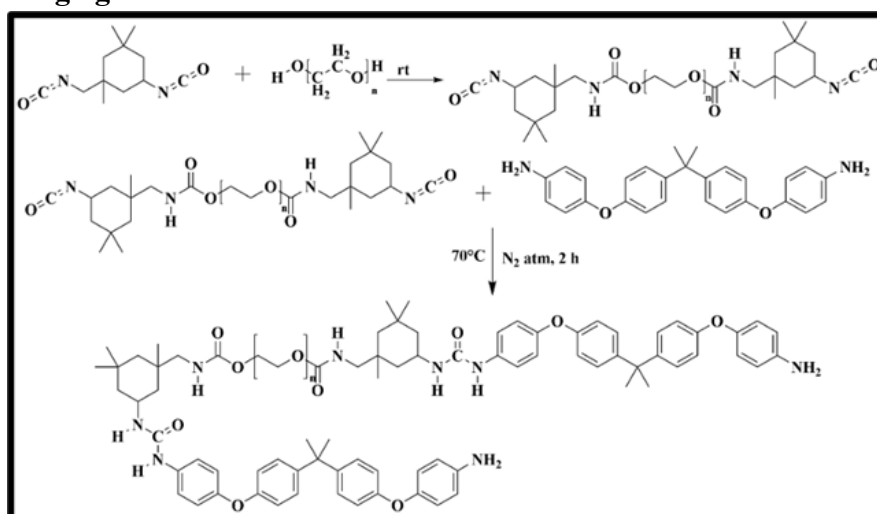


**Figure 13: Reaction scheme for the synthesis of PEG-4,4'-(4,4'-Isopropylidenediphenyl-1,1'-diylldioxy)dianiline-IPDI based curing agent**



## 2. Synthesis of PEG-Melamine-IPDI-based curing agent

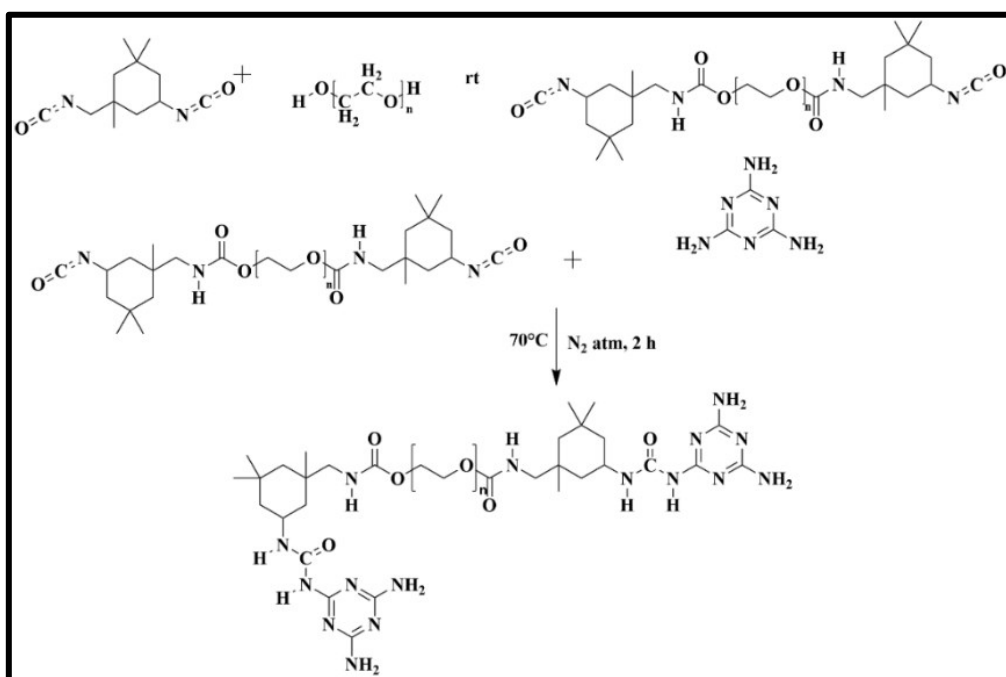


Figure 14: Reaction scheme for the synthesis of PEG-Melamine-IPDI-based curing agent

## 3. Synthesis of PEG-Hexamethylenediamine-IPDI based curing agent

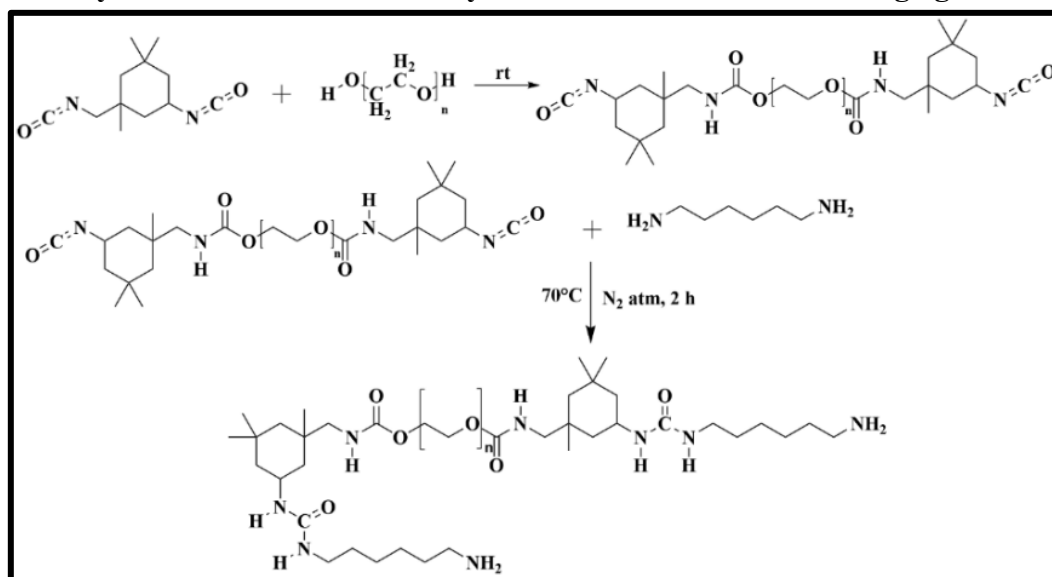


Figure 15: Reaction scheme for the synthesis of PEG-Hexamethylenediamine-IPDI based curing agent

### 4.3: Results and Discussion:

The physicochemical structure of the synthesized epoxy was analyzed to authenticate its proposed structure.

#### NMR study

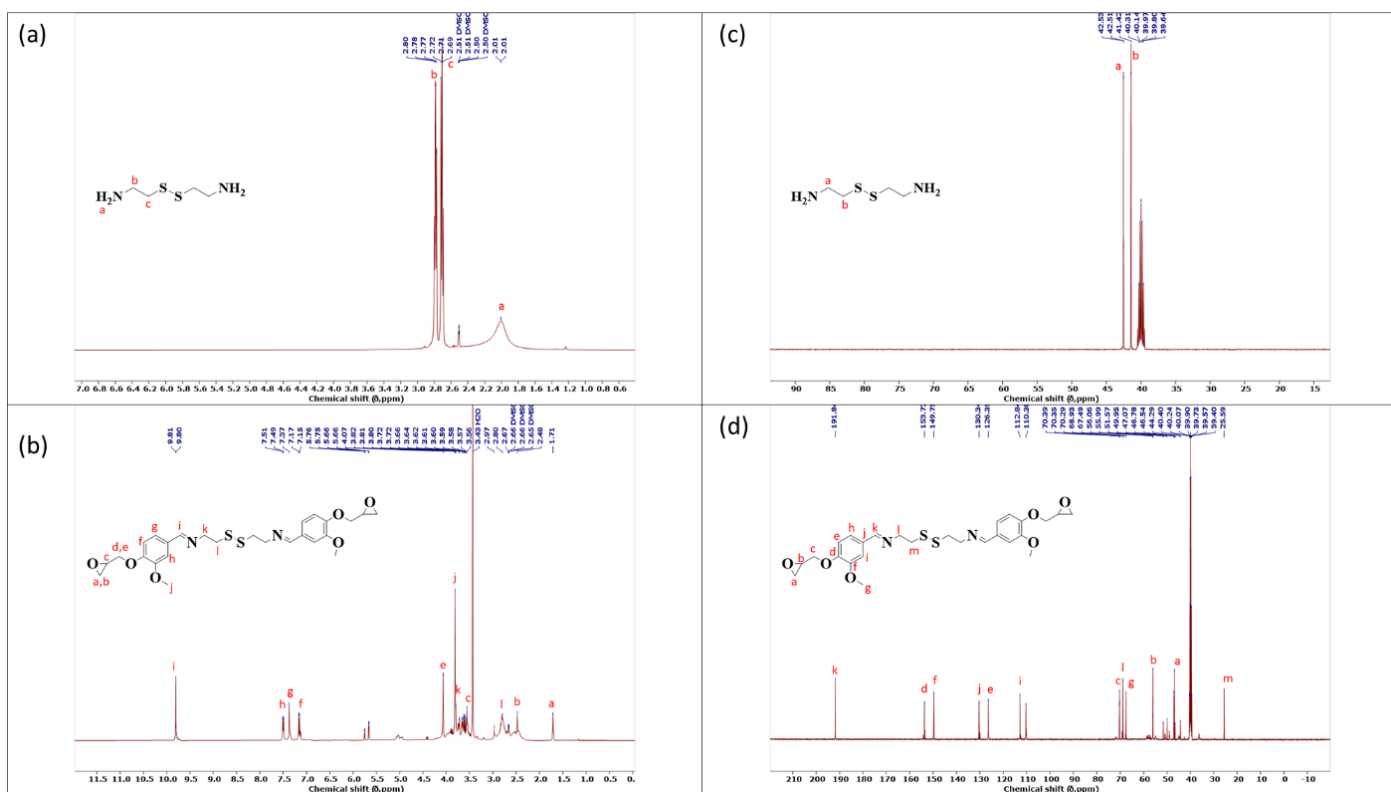


Figure 16:  $^1\text{H}$  NMR spectra of (a)Cystamine (b) cystamine based epoxy,  $^{13}\text{C}$  NMR spectra of (c)cystamine (d)cystamine based epoxy

Figure 17 shows the FTIR spectra of vanillin, the imine obtained from vanillin using cystamine (VCI), and the corresponding epoxy resin (VCIE). In the FTIR spectra characteristic absorption band at around  $3400\text{ cm}^{-1}$  corresponding to the OH group and peak at around  $1592\text{ cm}^{-1}$  corresponding to the C=O stretch appears in all four spectra. The shifting of the C=O peak from  $1665\text{ cm}^{-1}$  in vanillin to  $1642\text{ cm}^{-1}$  in VCI might be indicative of imide formation. The characteristic epoxy peak at  $914\text{ cm}^{-1}$  in VCIE confirms successful epoxidation.

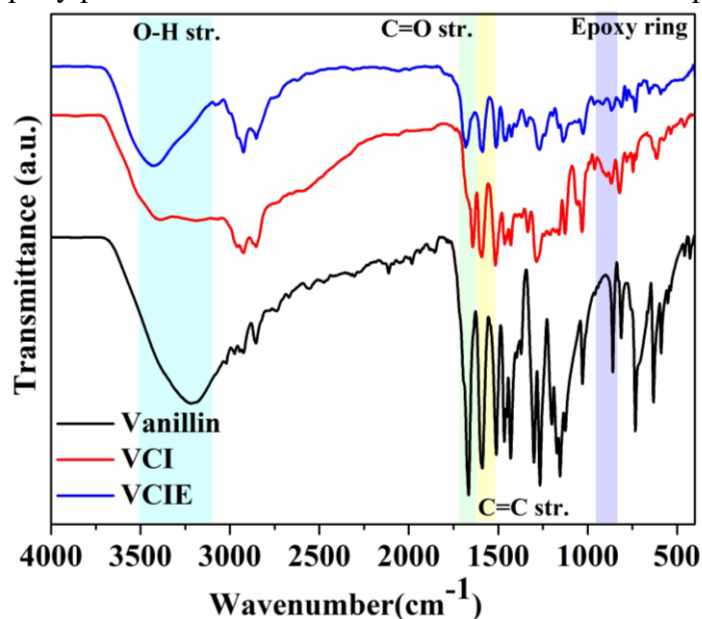


Figure 17: FTIR spectra of vanillin, vanillin-based imine, and its epoxy (VCIE)

### Mechanical property evaluation

The stress-strain curve along with the toughness of the thermosets prepared using cystamine is depicted in Figure 18. Further optimization is required to improve the mechanical properties of the thermoset.

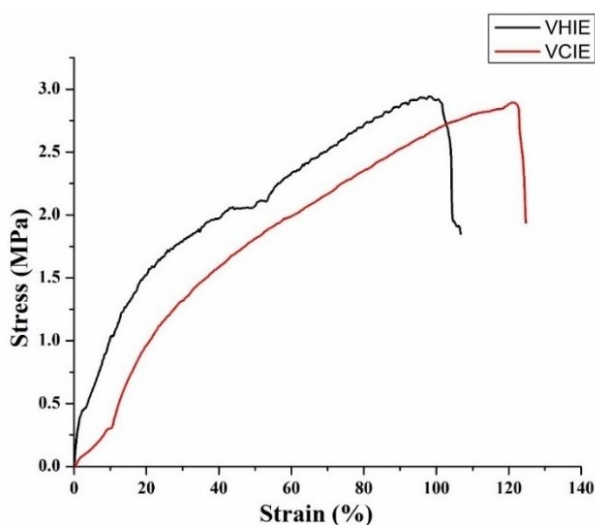


Figure 18: Stress-strain curve of epoxy cured with PAA

**4.4: Conclusion:** The synthesis of epoxy resins and curing agents was successfully completed, followed by an assessment of the compatibility between the epoxy resins and the curing agents. The combination of glycolic acid and 4,4'-Oxydianiline-based epoxy, as well as 2,2' Bis(hydroxymethyl)propionic acid and 4,4'-Oxydianiline-based epoxy, resulted in brittle thermosets. Additionally, low compatibility was observed between gallic acid-based epoxy and IPDI-based curing agents. Therefore, further work was carried out using gallic acid and PAA-based curing agents.

## 5. Chapter 3: Tailoring Thermomechanical Properties of UV-Shielding Biodegradable Epoxy Thermosets via Chain Length Modulation

**5.1.Purpose:** A series of flexible UV-shielding epoxy thermosets with tunable properties were prepared using gallic acid and varying lengths of PEGs.

### 5.2. Details of protocol/work done:

Gallic acid (GA) (>98%, molecular weight 170.12 g/mol), ethylene glycol (EG) (molecular weight 62.07 g/mol), poly(ethylene glycol) ( $M_n$  200 g/mol) (PEG 200), poly(ethylene glycol) ( $M_n$  400 g/mol) (PEG 400), poly(ethylene glycol) ( $M_n$  600 g/mol) (PEG 600), and para-toluene sulphonic acid (pTSA) were procured from SRL Pvt. Ltd., India and were used by overnight drying in a vacuum oven at 55 °C. Epichlorohydrin, sodium chloride (NaCl), sodium hydroxide (NaOH), and anhydrous sodium sulfate ( $Na_2SO_4$ ) were procured from Merck, India. Poly(amido amine) which was used as a hardener with a viscosity of 10-14 Pa s and an amine value of 5-7 eq./kg was offered by Asian Paints, India. Tetrahydrofuran (THF) and acetone were procured from S.D. Fine Chem Ltd, India, and were used post-distillation. Bacterial strains *Pseudomonas aeruginosa* (PA) and *Bacillus subtilis* (BS) for carrying out the

biodegradation study were provided by the Department of Molecular Biology and Biotechnology, Tezpur University, India.

### ***Synthesis of epoxy resins of GA esters with epichlorohydrin***

The GA ester-based epoxy resins were synthesized from the respective GA esters by the usual epoxide formation approach involving polycondensation between GA ester polyol and epichlorohydrin at 70 °C for 2 h with aqueous NaOH added dropwise being used as the base. GA ester (1 equiv.) and 24 equiv. of epichlorohydrin (relative to GA ester) were taken in a 100 mL round-bottomed flask (three-neck) equipped with a dropping funnel, an overhead mechanical stirrer, a thermometer, and an oil bath. An amount of 6 equiv. (relative to GA ester) of 5N aqueous NaOH solution was introduced to this reaction mixture dropwise maintaining the flow rate such that the pH of the reaction content was maintained at around 7.4 using a pressure-equalizing funnel (2-2.5 h). After the complete addition of NaOH solution, the reaction continued for another 2 h at 70 °C. The contents of the reaction mixture were then transferred to a separating funnel after the attainment of room temperature. The aqueous layer containing dissolved side products (like NaCl) formed during the reaction was siphoned out from the preferred organic layer. The latter was washed with 16% brine solution to break emulsions formed, if any, followed by washing a couple of times with fresh water to eliminate water-soluble impurities if any, along with the other precursors. The organic layer was then dissolved in THF and filtered. The desired epoxy resin was obtained by drying the filtrate at 70 °C under a vacuum by means of a rotary evaporator to withdraw spare epichlorohydrin and trapped water from the resin. The end products obtained were sticky viscous transparent light-brown masses coded as EP 0, EP 2, EP 4, and EP 6, respectively for the epoxy resins obtained from esters prepared using EG, PEG 200, PEG 400, and PEG 600. The plausible synthetic route is shown in Scheme 1.

**EP 2:** <sup>1</sup>H NMR (500 MHz, DMSO) δ 7.21, 7.09, 5.68, 4.57, 4.54, 4.32, 4.25, 4.23, 4.22, 4.14, 4.02, 4.01, 3.99, 3.83, 3.82, 3.81, 3.70, 3.69, 3.68, 3.64, 3.63, 3.61, 3.60, 3.60, 3.59, 3.57, 3.55, 3.53, 3.30, 2.82, 2.81, 2.74, 2.69, 2.60, 2.51, 2.40, 2.39, 2.37, 2.13, 2.12, 2.10, 1.70. <sup>13</sup>C NMR (126 MHz, DMSO) δ 165.66, 152.15, 147.74, 141.97, 125.17, 112.15, 108.85, 74.48, 72.55, 70.45, 70.33, 70.12, 69.07, 68.72, 67.46, 65.65, 64.60, 63.01, 60.67, 60.14, 50.15, 47.32, 46.80, 46.61, 44.08, 40.05, 39.96, 39.88, 39.79, 39.71, 39.63, 39.59, 39.46, 39.29, 39.12, 38.96, 25.47.

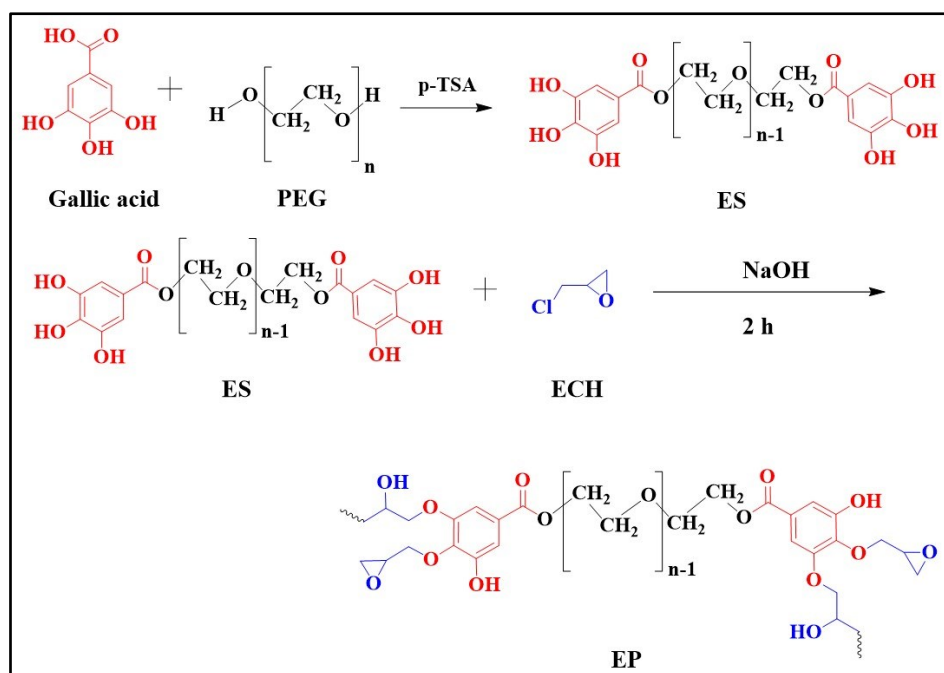


Figure 19: Plausible reaction scheme for the formation of gallic acid ester and its epoxy resin

### Curing of resin

To analyze the physical properties of the epoxy, they were converted to their thermoset form by curing with a nearly stoichiometric amount of hardener. Homogeneous mixtures of resins were prepared in a 25 mL beaker with the commercially available bio-based aliphatic curing agent PAA. The amount of resin and hardener to be mixed was estimated in terms of parts by weight of curing agent per hundred parts resin (phr) using amine hydrogen equivalent weight (AHEW) and epoxide equivalent weight (EEW) with the help of the following equations-

$$AHEW = \frac{\text{Molecular weight of amine}}{\text{Number of active hydrogens}} \quad (\text{eq. 1})$$

$$phr = \frac{AHEW \times 100}{EEW} \quad (\text{eq. 2})$$

The mixture was blended by physical hand stirring for around 5 min using a minimum volume of THF as the solvent at room temperature to obtain a homogenous mixture. The mixture was degassed to remove excess solvent and entrapped air in a vacuum desiccator which was then uniformly spread on tin plates and glass slides for carrying out impact resistance, scratch resistance, gloss, and chemical resistance tests. The epoxy-coated plates after becoming touch-free were cured and post-cured at a specific temperature for a specified period which was optimized by examining the swelling value of the prepared thermosets in THF. For optimal curing, this value should lie between 20 and 30%.

The swelling value of the thermosets was determined by calculating the change in weight of the thermoset after being immersed in THF solvent for 48 h. The swelling value was evaluated using the following equation-

$$\text{Swelling value (\%)} = \left[ \frac{w_s - w_d}{w_d} \right] \times 100 \quad (\text{eq. 3})$$

where  $w_s$  and  $w_d$  are the weight of the swollen and dry thermosets.

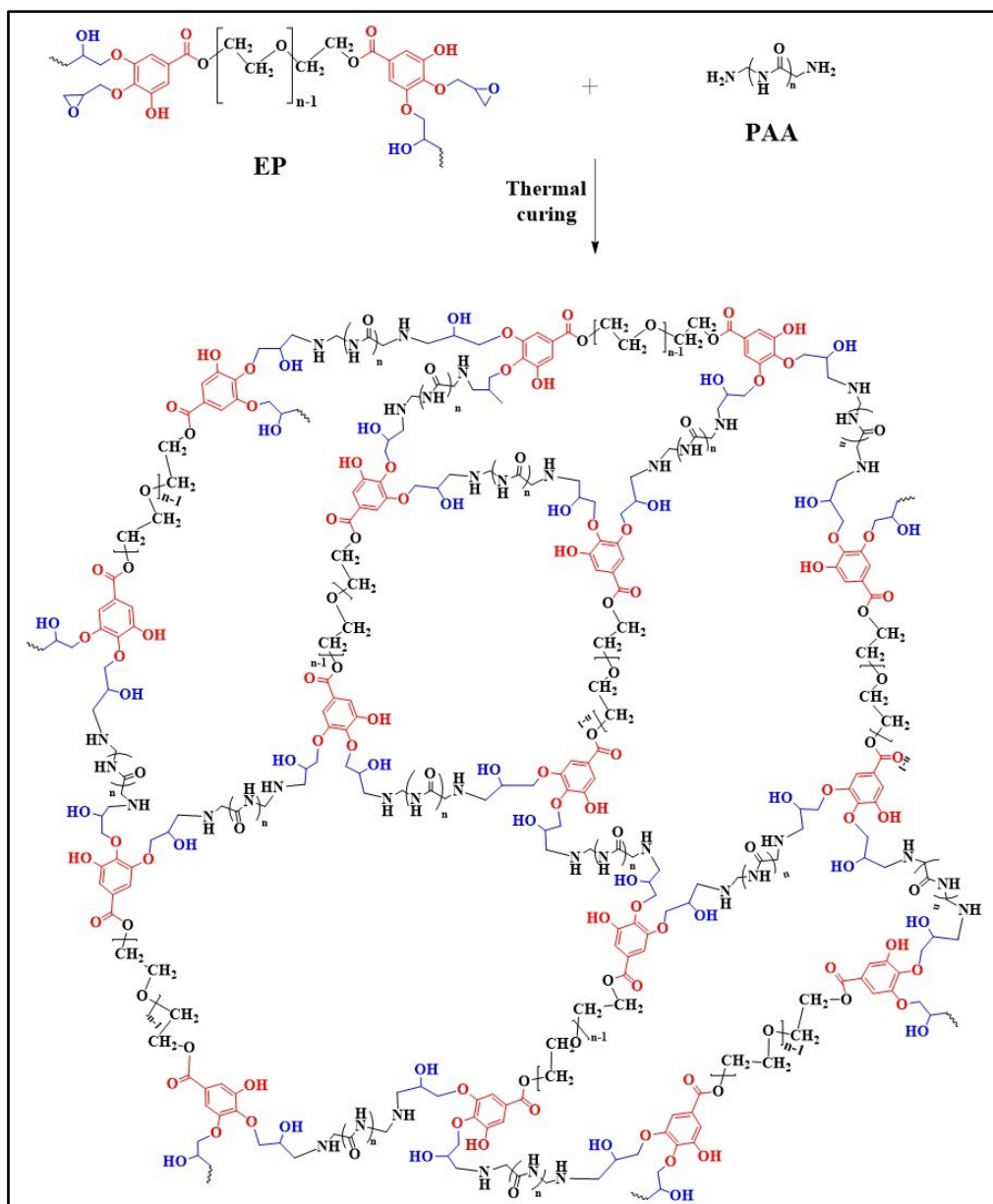


Figure 20: Crosslinking of EP with PAA to obtain the thermoset (ET)

**Instrumentation and Methods:** As described in details of protocol of Chapter 1.

### 5.3. RESULTS AND DISCUSSION

**Structural analysis:** The physicochemical structure of the synthesized epoxy was analyzed to authenticate its proposed structure.

#### Synthesis and characterization of epoxy prepolymers

Epoxy prepolymers were prepared in a two-step synthetic procedure as depicted in Figure 19. Melt polycondensation of GA with an excess of desired diol (EG or PEG with varying chain lengths) with the removal of water using a vacuum pump resulted in the corresponding esters bearing hydroxyl groups. Glycidylation of the hydroxy-branched esters in an alkaline medium (pH 7.4) with excess epichlorohydrin gave the corresponding epoxy prepolymers. The physicochemical structure of the synthesized epoxy was analyzed to authenticate its proposed structure using FTIR,  $^1\text{H}$  NMR,  $^{13}\text{C}$  NMR, and GPC.

**Fourier transform infrared spectroscopy (FTIR) study:** Figure 21(a) shows the FTIR spectra of GA, the ester obtained from GA using PEG 200 (ES 2), the corresponding epoxy resin of the ester (EP 2), and the cured thermoset (ET 2). In the FTIR spectra characteristic absorption band near  $3400\text{ cm}^{-1}$  corresponding to the OH group and peak near  $1619\text{ cm}^{-1}$  corresponding to the C=O stretch appear in all four spectra. The narrowing of the OH peak as well as its shifting from  $3298\text{ cm}^{-1}$  in GA to  $3437\text{ cm}^{-1}$  in ES 2, shifting of the C=O peak, the appearance of characteristic C-O-C stretch at  $1091\text{ cm}^{-1}$  in ES 2 which is absent in GA might be indicative of esterification taking place.

The characteristic epoxy peak at  $914\text{ cm}^{-1}$  in EP 2 is indicative of successful epoxidation. The two absorption peaks at  $2921\text{ cm}^{-1}$  and  $2856\text{ cm}^{-1}$  are assigned to aromatic and aliphatic C-H stretching, respectively. The C-O-C stretching absorption peaks for ether and oxirane appear at  $1091\text{ cm}^{-1}$  and  $864\text{ cm}^{-1}$ , respectively. Peaks at  $1601\text{--}1665\text{ cm}^{-1}$  and  $1207\text{--}1271\text{ cm}^{-1}$  correspond to aromatic C=C bond and phenolic C-O group, respectively.

Figure 21(b) shows the FTIR spectra of all the epoxy resins prepared using esters of varying chain lengths. All the spectra have the characteristic C-O stretching peak of the epoxy ring at  $914\text{ cm}^{-1}$  indicating successful epoxide formation.

The curing of the epoxy resin was analyzed by attenuated total reflectance analysis of the resulting thermosets. The characteristic epoxy peak at  $914\text{ cm}^{-1}$  in the cured thermosets completely vanished indicating a significant decrement in the number of epoxy rings due to the opening up of the epoxy rings in the resin, while crosslinking with the hardener.

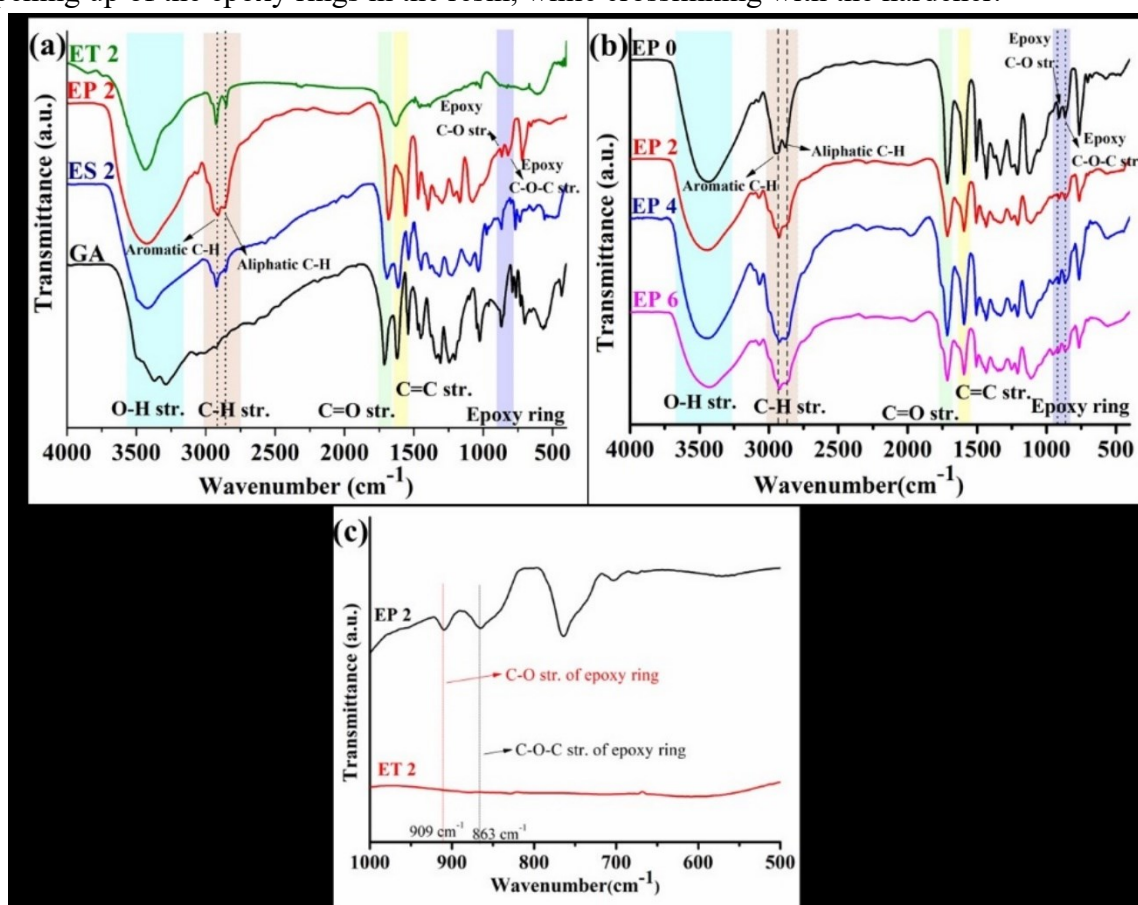


Figure 21: (a) FTIR spectra of Gallic acid (GA), Gallic acid ester (ES), Epoxy of gallic acid ester (EP) and its thermoset (EH), (b) All the epoxy resins prepared using esters of varying chain lengths, and (c) Enlarged spectra of epoxy resin and corresponding thermoset depicting curing process



Figure 1 displays the  $^1\text{H}$  and  $^{13}\text{C}$  NMR spectra of poly(2,6-bis(4-hydroxyphenyl)-2,5-dioxane-1,4-dione) (PBD). The figure is divided into four panels (a, b, c, d) showing chemical structures and corresponding spectra.

**(a)  $^1\text{H}$  NMR spectrum:** The chemical structure of PBD is shown with protons labeled a through f. The spectrum shows peaks corresponding to these labels: a (aromatic H, ~7.1 ppm), b (aromatic H, ~7.1 ppm), c (aromatic H, ~7.1 ppm), d (CH<sub>2</sub> in repeat unit, ~4.1 ppm), e (CH<sub>2</sub> in repeat unit, ~4.1 ppm), and f (CH<sub>2</sub> in repeat unit, ~4.1 ppm). The x-axis is chemical shift (ppm) from 1.0 to 14.0.

**(b)  $^{13}\text{C}$  NMR spectrum:** The chemical structure of PBD is shown with carbons labeled a through g. The spectrum shows peaks corresponding to these labels: a (aromatic C, ~146 ppm), b (aromatic C, ~146 ppm), c (aromatic C, ~146 ppm), d (CH<sub>2</sub> in repeat unit, ~120 ppm), e (CH<sub>2</sub> in repeat unit, ~120 ppm), f (CH<sub>2</sub> in repeat unit, ~120 ppm), and g (CH<sub>2</sub> in repeat unit, ~120 ppm). The x-axis is chemical shift (ppm) from 10 to 190.

**(c)  $^1\text{H}$  NMR spectrum:** The chemical structure of PBD is shown with protons labeled a through n. The spectrum shows peaks corresponding to these labels: a (aromatic H, ~7.1 ppm), b (aromatic H, ~7.1 ppm), c (aromatic H, ~7.1 ppm), d (CH<sub>2</sub> in repeat unit, ~4.1 ppm), e (CH<sub>2</sub> in repeat unit, ~4.1 ppm), f (CH<sub>2</sub> in repeat unit, ~4.1 ppm), g (CH<sub>2</sub> in repeat unit, ~4.1 ppm), h (CH<sub>2</sub> in repeat unit, ~4.1 ppm), i (CH<sub>2</sub> in repeat unit, ~4.1 ppm), j (CH<sub>2</sub> in repeat unit, ~4.1 ppm), k (CH<sub>2</sub> in repeat unit, ~4.1 ppm), l (CH<sub>2</sub> in repeat unit, ~4.1 ppm), m (CH<sub>2</sub> in repeat unit, ~4.1 ppm), and n (CH<sub>2</sub> in repeat unit, ~4.1 ppm). The x-axis is chemical shift (ppm) from 1.0 to 14.0.

**(d)  $^{13}\text{C}$  NMR spectrum:** The chemical structure of PBD is shown with carbons labeled a through n. The spectrum shows peaks corresponding to these labels: a (aromatic C, ~146 ppm), b (aromatic C, ~146 ppm), c (aromatic C, ~146 ppm), d (CH<sub>2</sub> in repeat unit, ~120 ppm), e (CH<sub>2</sub> in repeat unit, ~120 ppm), f (CH<sub>2</sub> in repeat unit, ~120 ppm), g (CH<sub>2</sub> in repeat unit, ~120 ppm), h (CH<sub>2</sub> in repeat unit, ~120 ppm), i (CH<sub>2</sub> in repeat unit, ~120 ppm), j (CH<sub>2</sub> in repeat unit, ~120 ppm), k (CH<sub>2</sub> in repeat unit, ~120 ppm), l (CH<sub>2</sub> in repeat unit, ~120 ppm), m (CH<sub>2</sub> in repeat unit, ~120 ppm), and n (CH<sub>2</sub> in repeat unit, ~120 ppm). The x-axis is chemical shift (ppm) from 10 to 190.

The  $^1\text{H}$  NMR (DMSO) spectrum of ES 2 is shown in Figure 22(a). The absence of a peak at around 12 ppm corresponding to the  $-\text{COOH}$  group of GA is indicative of successful esterification. The small broad peak at  $\delta=9.38$  ppm and peak at  $\delta=8.74$  ppm appears due to the hydroxyl protons at meta and para positions relative to the carbonyl group and the lower intensity of these peaks might be due to H-bonding between two different synthesized ester moieties. The peak at  $\delta=6.95$  ppm is expected to be due to protons directly attached to the phenyl ring of GA moiety in the ester molecule. The peaks at  $\delta=4.48$  ppm and  $\delta=4.27$  ppm are expected to appear due to the methylene protons. The peak at  $\delta=2.51$  ppm appeared due to the solvent used in NMR analysis, DMSO- $\text{d}_6$ . The peak at  $\delta=3.56$  ppm appeared due to residual water which was released during the reaction. The other peaks might be due to unused catalyst p-TSA, unreacted EG, and other impurities.

The  $^1\text{H}$  NMR (DMSO) spectrum of EP is shown in Figure 22(c). The peaks at  $\delta=7.21$  ppm and 6.97 ppm appear due to the hydroxyl group attached to the aromatic ring and protons



at the ortho position to C attached to a carbonyl group. Peaks at  $\delta=4.57$ , and  $3.55$  ppm are due to protons attached to the alkyl chain of PEG moiety. Peaks at  $\delta=4.02$ , and  $3.7$  ppm are due to protons attached to C next to the oxirane ring of the glycidyl group. The peak at  $\delta=3.3$  ppm is due to the CH proton of the oxirane ring. Peaks at  $\delta=2.74$ , and  $2.69$  ppm are due to  $\text{CH}_2$  protons of the epoxy ring. Other peaks might be due to the opening up of the oxirane ring and other impurities.

The  $^{13}\text{C}$  NMR (DMSO) spectrum of EP is shown in Figure 22(d). The peak at  $\delta=165.66$  ppm is due to the carbonyl C. Peak at  $\delta=152.15$  ppm and  $147.74$  ppm appear due to aromatic Cs at meta and peak at  $\delta=141.97$  ppm due to aromatic C at para positions respectively relative to the C attached to the carbonyl group. The peak at  $\delta=125.17$  ppm is due to the aromatic C linked to the carbonyl group. The peak at  $\delta=108.85$  ppm is due to the unsubstituted aromatic Cs. Peaks at  $\delta=74.48$  ppm and  $70.12$  ppm are due to the Cs next to the oxirane ring. Peaks at  $\delta=69.07$ , and  $67.46$  ppm are due to the alkyl Cs of the PEG moiety. Peaks at  $\delta=50.15$ , and  $44.08$  ppm are due to the Cs of the oxirane ring. The other peaks of lower intensity might be due to the opening of the oxirane ring and other impurities.

### Physical and mechanical properties

The physical properties including color, transparency, gloss, specific gravity, etc. of the epoxy thermosets were determined and tabulated in Table 3. With the increase in cross-linking density between the functionalities, tensile strength increases resulting in a subsequent decrease in elongation at break. The molecular weight of the polymeric network also affects the physical properties. The stress-strain profile recorded for the series of epoxy thermosets with varying chain lengths is shown in Figure 23(a).

A significant decrease in tensile strength and an increase in elongation at break was observed with the increase in ester chain length. The higher value of tensile strength is due to higher aromatic content per unit molecule. Also, the presence of polar functionalities in GA moiety as well as amine-based aliphatic hardener enhances the crosslinking density by intra and intermolecular secondary interactions that played a crucial role in determining the tensile properties. So, with the decrease in the amount of gallic acid moiety per unit mass of the resin from EP 0 to EP 6 resulted in a gradual decrease in the tensile strength of the thermoset due to the lowering of the aromatic and polar groups content per unit volume of the thermoset. The increase in chain length from EP 0 to EP 6 provided flexibility to the system thus increasing the elongation at break. The Young's modulus value calculated from the stress-strain curve showed a decrease with an increase in the ester chain length. The toughness of any material, which is the product of tensile strength and elongation at break determined by integrating the area under the stress-strain curve was observed to be highest for ET 2 ( $380.4 \text{ J/m}^3$ ) thermoset obtained from the epoxidation of gallic acid ester prepared from PEG 200.

The impact resistance test evaluates the ability of a material to resist sudden flexural shock applied to it without breaking or cracking it. All the prepared thermosets exhibited the instrument's limiting value of impact strength ( $19.3 \text{ kJ/m}^2$ ).

Scratch hardness values of cured epoxy thermosets decreased with the increase in chain length, this observation can be attributed to the decrease in cross-linking density with the increase in chain length.

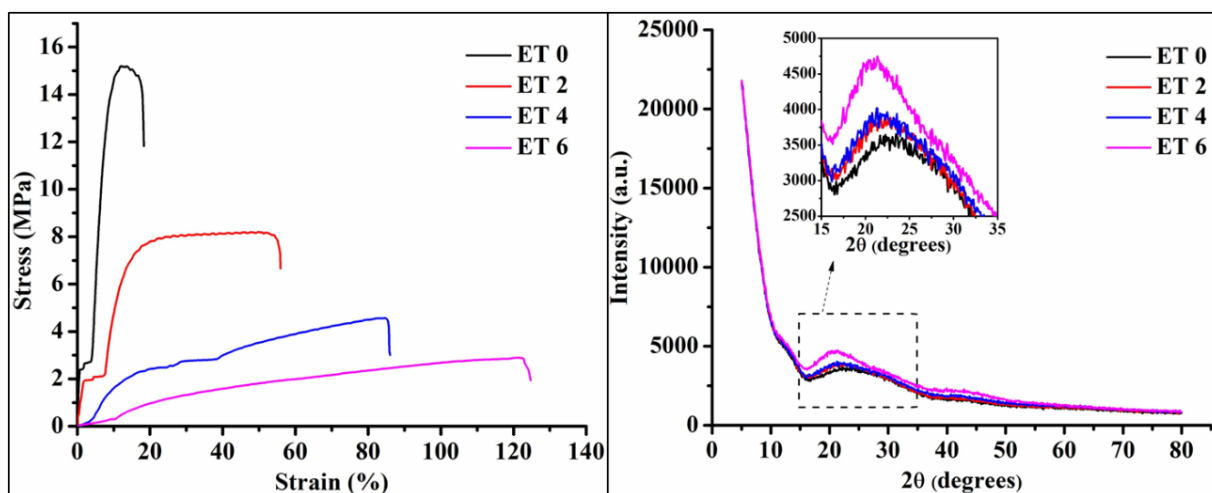


Figure 23: (a) Stress-strain curves and (b) PXRD pattern of cured epoxy thermostets

Table 12: Mechanical properties of the epoxy resins along with their cured thermostets

Sample Code	EP 0	EP 2	EP 4	EP 6
Tensile strength (MPa)	15.18	8.19	4.56	2.89
Elongation at break (%)	16.91	53.98	84.8	121.7
Toughness (J/m <sup>3</sup> )	193.8	380.4	262.1	232.7
Young's Modulus (GPa)	1.50	0.43	0.17	0.05
Impact resistance (kJ/m <sup>2</sup> )	>19.3	>19.3	>19.3	>19.3
Gloss (60°)	60.2	80.86	76	79
Scratch resistance (kg)	7.5	7	6.5	5.5
Specific gravity of resin	1.32	1.21	1.14	1.11
Specific gravity of thermostet	1.54	1.36	1.27	1.21

#### Viscosity measurement

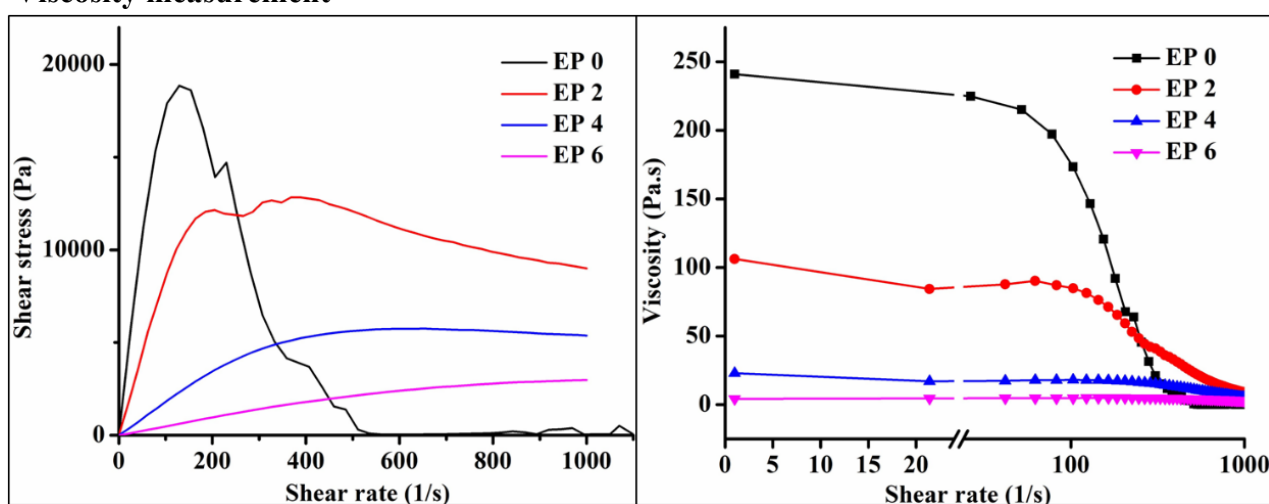


Figure 24: (a) Shear stress and (b) viscosity of the epoxy resins as a function of shear rate

To comprehend the processability and structure-property relation of epoxy resins, knowledge of which is critical for their industrial applications, a rheology study was performed. The

rheological properties of a resin depend on various factors like the presence of polar functionality, molecular weight distribution, monomer distribution, the presence of hydrophobic and hydrophilic functionalities, the macrostructure of the chains, etc. Figures 24(a) and 24(b) depict the variation of shear stress and viscosity of the epoxy resins as a function of shear rate. The viscosities of the synthesized epoxy resins were measured at 25 °C (Figure 24) with the help of a rheometer. It was observed that resins exhibit Newtonian behavior up to a certain shear rate (critical shear rate) which marks the initiation of the shear thinning transition. An increment in the value of the critical shear rate was observed with an increase in the chain length of the epoxy prepolymer resin. However, shear thinning is observed within a small range of shear rates (from 50-700 s<sup>-1</sup>) after which the resins attain Newtonian behavior over all the measured frequency ranges. The initial shear viscosity,  $\eta_0$  was observed to decrease with an increase in chain length. These observations can be explained based on the alignment of polymeric chains under shear stress. With an increase in polymeric chain length, chain entanglement increases, and hence packing density decreases, decreasing the ordered structure and hence viscosity decreases. Thus EP 4 and EP 6 resins with low viscosity can be used as reactive diluents for highly viscous resins.

### XPS study

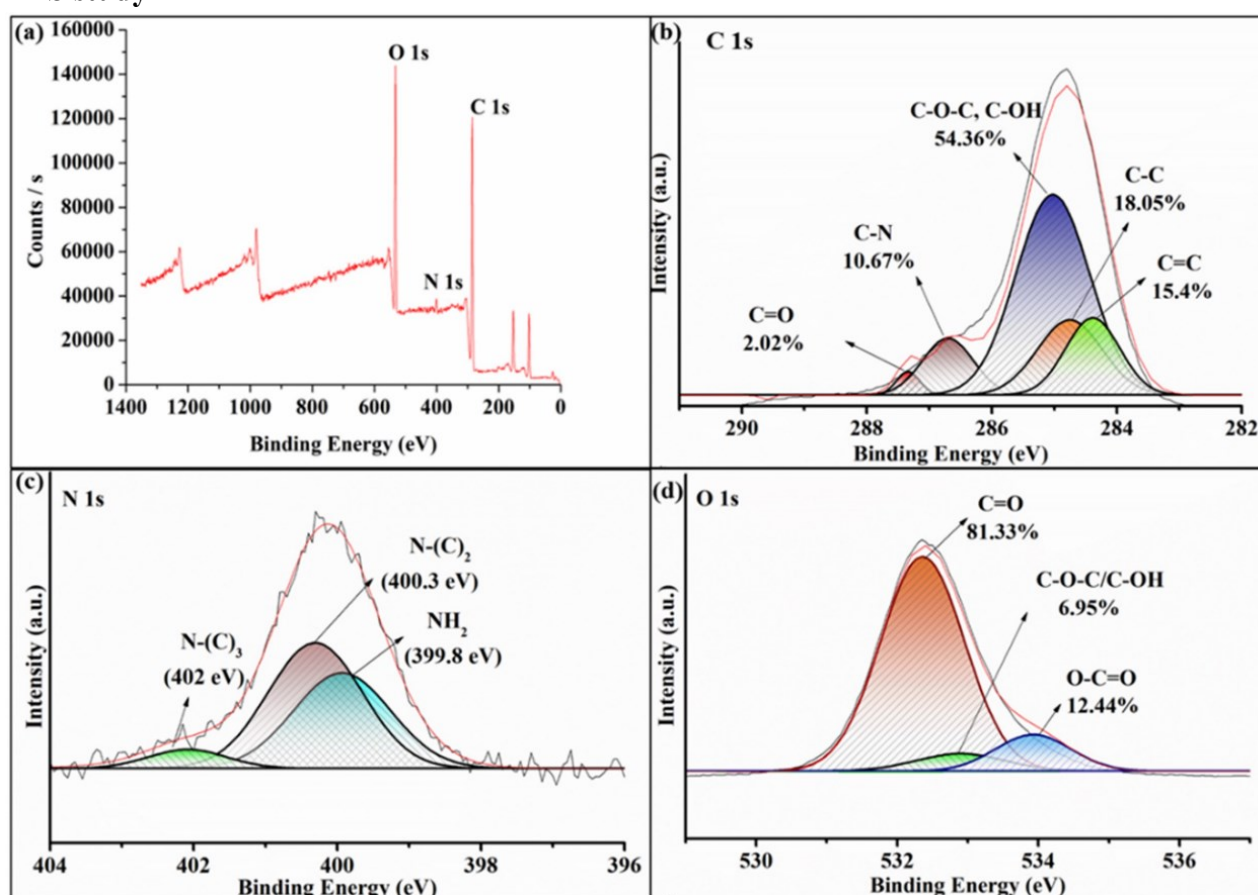


Figure 25:(a) XPS survey spectra of the epoxy thermoset ET 2 and their high-resolution deconvoluted spectra of (b) C 1s, (c) N 1s, and (d) O 1s peaks.

XPS analysis was conducted to determine the elemental composition as well as their chemical states, electronic structure, and density of the electronic states in the epoxy thermoset (ET 2,

Figure 25). The atomic composition of the thermoset surface as determined by 1s peak fitting revealed the following surface composition: 52.61 at % C, 3.98 at % N, and 43.4 at % O.

The C1s, N1s, and O1s spectra of the epoxy thermoset are presented in Figure 25. The deconvoluted C1s spectrum exhibits five peaks at 287.4, 286.7, 285.02, 284.75, and 284.37 eV which can be attributed to C=O, C-N, C-OH or C-O-C, C-C, and C=C bonds, respectively. Similarly, the deconvoluted N1s spectrum exhibits three peaks at 402, 400.3, and 399.8 eV which are assigned to tertiary, secondary, and primary nitrogen, respectively. The deconvoluted O1s spectrum exhibits three peaks at 532.3, 532.9, and 533.9 eV which are assigned to C=O, C-O-C or C-OH, and O-C=O bonds, respectively. Thus, the XPS analysis gives a broad overview of the elemental and chemical composition of the cured thermosets.

### XRD study

X-ray diffractograms of the thermosets are shown in Figure 23(b), which reveal the absence of any sharp peak indicating the amorphous nature of the thermosets.

### Chemical resistance studies

The pristine polymer does not show excellent chemical resistance which may be due to the hydrolyzable ester group present in the structure of thermosets.

**Table 13: Chemical resistance studies for 30 days of the epoxy thermosets**

Type of media	Weight Changes (%)			
	EP 0	EP 2	EP 4	EP 6
<b>Alkali (pH=7.5)</b>	3.68	3.27	2.29	2.17
<b>NaCl (10%)</b>	0.58	0.72	0.85	0.80
<b>HCl (pH=6)</b>	1.88	1.96	2.75	2.82
<b>Tap Water</b>	0.20	0.24	0.37	0.51
<b>Ethanol (10%)</b>	0.95	0.71	0.73	0.54

**Thermal  
thermoset**

**study of the epoxy**

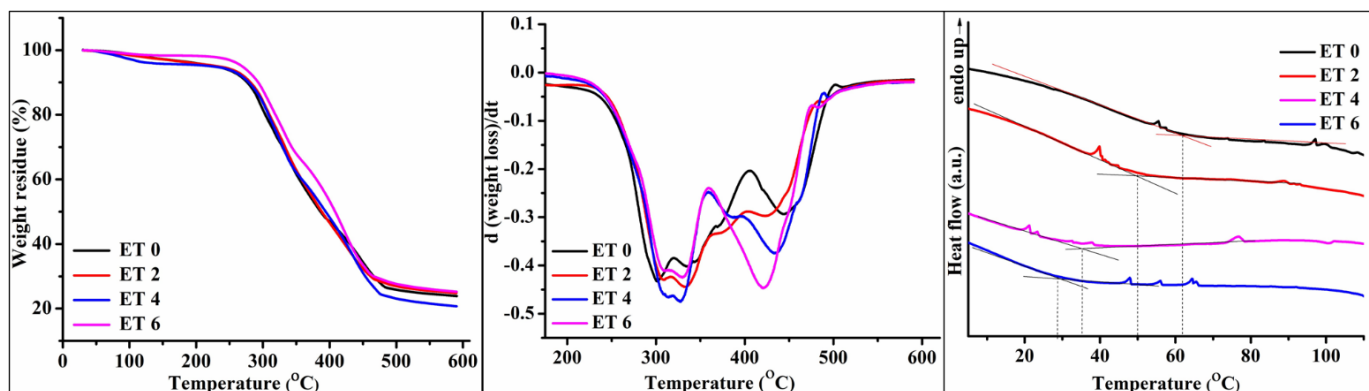


**Figure 26: (a) TGA thermograms (b) DTG curves indicating three-stage degradation, and (c) DSC curves displaying glass transition temperatures for the prepared epoxy thermostosets**

Thermostability is a significant characteristic of epoxy thermostosets as it extends the end-use of material across a broad range of temperatures. The thermogravimetric analysis measures the change in weight as a function of temperature. The analysis was conducted within the 30–600 °C temperature range. The TGA thermograms as elucidated in Figure 26(a) indicate no significant effect of ester chain length on the thermal stability of the cured thermostosets. The thermostosets exhibited three-stage degradation, the initial 4–7% degradation can be attributed to the elimination of small molecules such as THF, water, and other volatiles trapped inside the crosslinked polymeric network. The real degradation commenced ahead of 230 °C where the first stage degradation ranging from 236 °C to 320 °C, might correlate to the cleavage of ester bonds and other less thermostable bonds. The next stage of degradation ranging from 323 °C to around 360 °C might be due to the decomposition of cyclic and other relatively more thermostable moieties and amide linkages present in PAA which was used as the curing agent. The third stage of degradation ranging from around 400 °C to 470 °C might be due to the decomposition of aromatic rings of GA. The TGA thermograms display weight residue values of 24%, 25%, 21%, and 25% for ET 0, ET 2, ET 4, and ET 6, respectively. The values of thermal degradation temperature at 10%, 50%, and 70% weight loss ( $T_{10\%}$ ,  $T_{50\%}$ , and  $T_{70\%}$ , respectively) are listed in Table 5.

The value of glass transition temperature, an important property of amorphous polymers, depends on various factors like cross-linking density, presence of polar groups, length of side chains, etc. DSC thermograms as depicted in Figure 26(c) indicate the glass transition temperature of the cured epoxy thermostosets. It can be observed that the value of  $T_g$  increases with a decrease in the chain length which might be due to a denser network and reduced flowability in polymers of shorter chain length due to their higher cross-linked structures. ET 0 with the shortest chain length exhibited the highest  $T_g$  value amongst all the thermostosets.

**Table 14: Weight loss ( $T_{wt\%}$ ) of the cured thermosets along with their percent char residue at 600°C**

Epoxy Resin	$T_{10\%}$	$T_{50\%}$	$T_{70\%}$	% Char at 600 °C	$T_g$ (°C)
<b>EP 0</b>	275	385	466	24	29
<b>EP 2</b>	278	389	463	25	35
<b>EP 4</b>	280	393	453	21	50
<b>EP 6</b>	291	408	462	25	62

### Transparency and UV shielding performance of epoxy thermosets

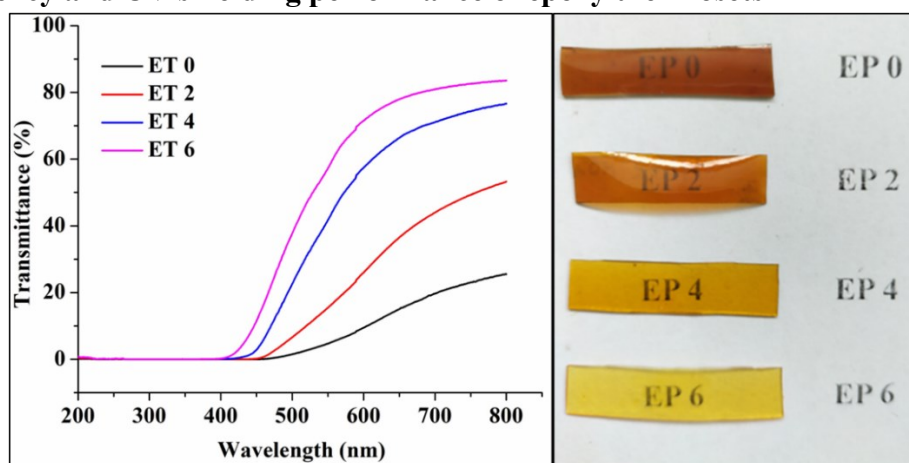


**Figure 27: (a) UV transparency curve of the prepared thermoset in the UV-vis range and (b) digital photographs of the thermosets**

The transparency of any material depends on its potential to transmit visible light across it which in turn depends on the ability of the material to scatter the absorbed light within the material. The more the scattering of light within the material, the more distorted and diminished the image of a through-seeing object will be (transparency decreases). The scattering is diminished in isotropic materials but increases in anisotropic crystalline materials resulting in usually translucent or opaque crystalline polymers.

Transmittance values for the epoxy thermosets with different chain lengths were recorded across a wavelength range of 200–800 nm and the corresponding transmittance curves are shown in Figure 27(a). A digital image of paper with sample codes printed, with and without the thermosets placed over the respective sample codes is also displayed in Figure 27(b). The transparency of the thermosets ET 6 is notably the highest at 83.5% in the visible region, followed by ET 4 at 76.5%, ET 2 at 53.4%, and ET 0 at 25.86%. An increase in the number of chromophores and auxochromes increases the absorption of visible light at frequencies corresponding to the excitation energy of the bonding electrons. Gallic acid and hence aromatic ring content per unit volume of the thermoset is higher in shorter chain length epoxy prepolymers. These aromatic rings act as chromophores with other conjugated bonds acting as auxochromes absorb strongly in the visible region, thus reducing the amount of transmitted light in case of shorter chain length polymeric thermosets as compared to their longer chain homologues. This is also the cause of greater UV-shielding capability in shorter chain length



polymers as observed in the figure 27(a). All the developed thermosets exhibited a transmittance of 0% in the UV spectral range of 0-390 nm. Among all the thermosets EP 0 and EP 2 exhibited obvious UV-blocking ability across the full UV range (200-400 nm) to 456 nm and 439 nm respectively, while EP 4 and EP 6 exhibited 0% transmittance from 200 to 397 and 391 nm respectively. The results obtained indicate that UV-shielding capability increases with a decrease in chain length. Non-absorption in the UV region broadens the applicability of the thermosets in the field of developing UV-shielded coatings.

### Biodegradation study

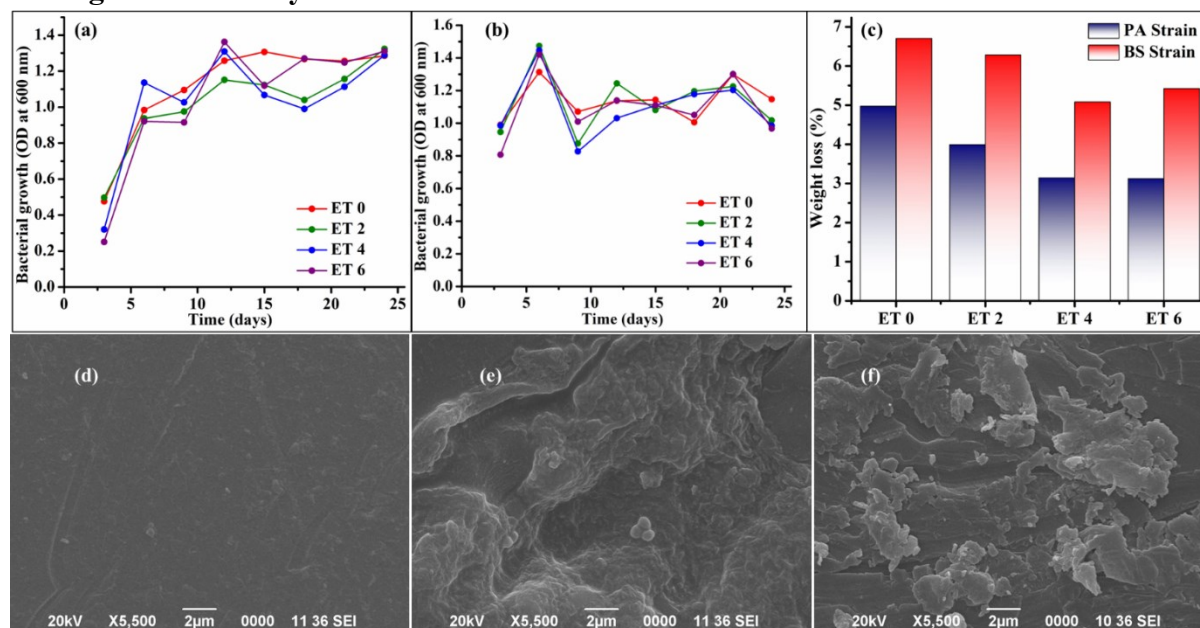


**Figure 28:** Optical density curves of (a) BS strain and (b) PA strain measured against time for a duration of 25 days (c) Weight loss (%) profiles, SEM images of the thermosets (d) before and after degradation test using (e) BS and (f) PA strain.

The biodegradation study was conducted on the cured thermosets by assessing the microbial growth curve based on optical density measurement of the bacterial culture medium. Two bacterial strains were employed, the gram-positive BS strain and the gram-negative PA strain using the standard McFarland turbidity method for a period of 25 days. The OD curve of the BS culture medium as depicted in Figure 28(a) shows a log phase after a period of 3 days where a rapid increase in the optical density of the medium is observed which indicates rapid bacterial cell growth. The medium then enters a stationary phase after 15 days when maximum cell density is reached in the culture, the antibacterial property of gallic acid might also be a potential factor. In the case of PA strain, the lag phase is insignificant while a rapid increase in OD is observed (the log phase) for a fleeting period of 6 days after which it enters the stationary phase followed by the decline phase. The significant antibacterial activity of gallic acid which is more effective against the PA strain than the BS strain might be a plausible explanation for better biodegradation in the BS strain as compared to the PA strain under identical environmental factors as observed from the weight loss profile (Figure 28(c)).

The SEM analysis of the thermoset (ET 2) was carried out to study for morphological changes before and after exposure of the thermosets to bacterial medium. From Figure 28, it can be

observed that the uniform surface of the thermoset (Figure 28(d)) eroded due to bacterial degradation (Figure 28(e) and (f)).

5.4. **Conclusion:** Highly flexible, biodegradable, bio-based epoxy resins of varying chain lengths with UV shielding ability were synthesized from GA-based esters and a bio-based curing agent, PAA. The comprehensive study suggested a significant effect of the chain length of the diols on the thermomechanical properties of the developed thermosets. The decrease in cross-linking density with the increase in chain length was observed to be responsible for the majority of observed thermomechanical property trends. Variations in chain length provided an important tool to alter various properties of the thermosets such as their glass transition temperature and tensile strength which were observed to decrease with an increase in the chain length. The viscosity of the uncured epoxy resins can also be controlled as a function of chain length which was observed to decrease with an increase in chain length.

## **6. Chapter 4: Epoxy thermosets with self-healing and self-cleaning properties synthesized using the Diels-Alder reaction and functionalized ZnO nanoparticles.**

6.1. **Purpose:** To develop a epoxy resin with self healing and self-cleaning properties.

6.2. **Details of protocol/workdone:**

### **Materials**

Furfuryl alcohol (FAL, 99%), 1,10-(methylenedi-1,4-phenylene) bismaleimide (BMI, 98%) were purchased from Sigma Aldrich. 2,2'-Disulfanediyl diethanamine dihydrochloride (Cystamine dihydrochloride) was procured from BLD pharm. Epichlorohydrin, sodium chloride (NaCl), sodium hydroxide (NaOH), and anhydrous sodium sulfate ( $\text{Na}_2\text{SO}_4$ ) were procured from Merck, India.

### **Methods**

#### ***Synthesis of furfuryl glycidyl ether***

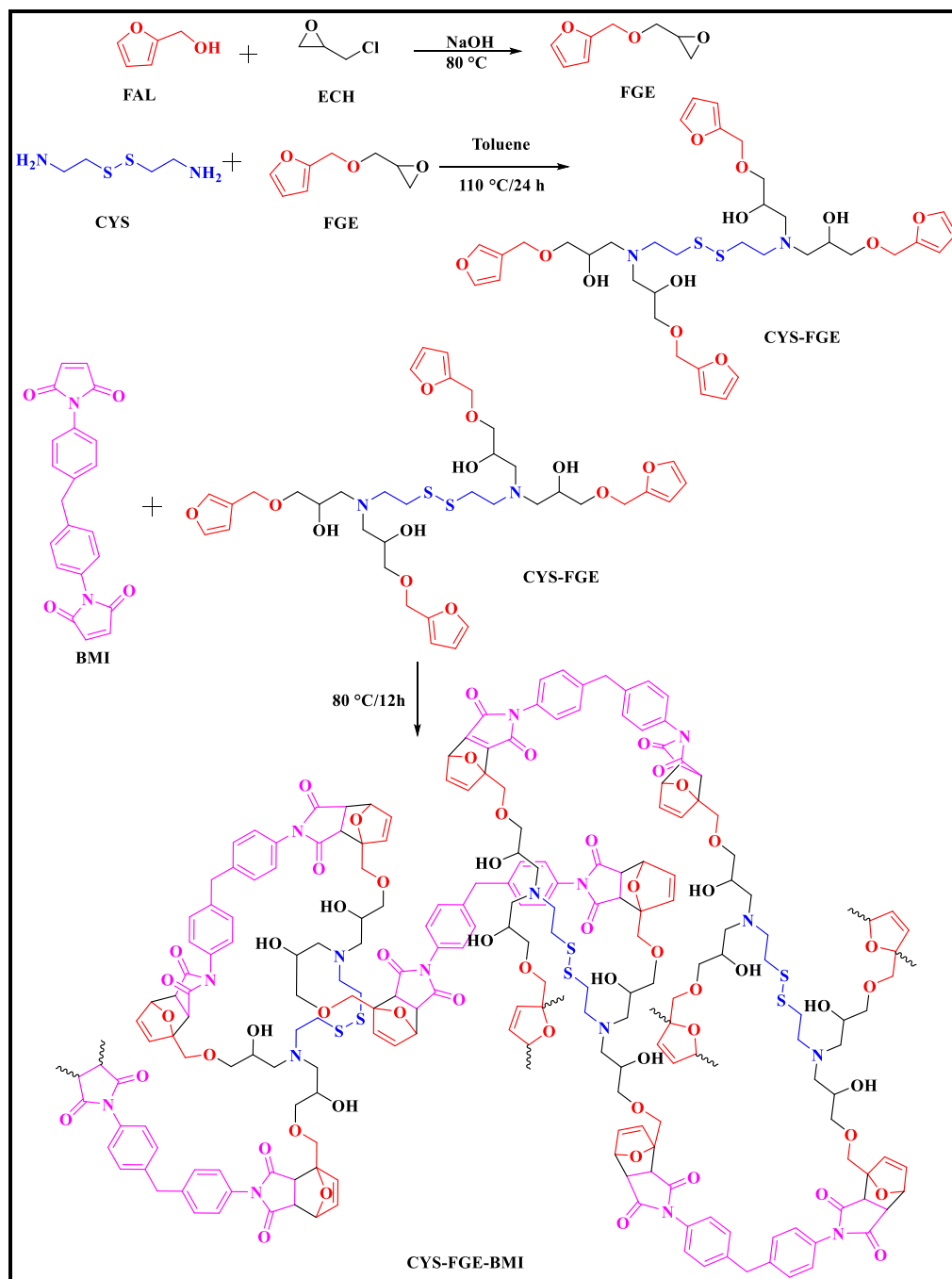
The FAL-based epoxy resin was synthesized by the usual epoxide formation approach involving polycondensation between FAL and epichlorohydrin with aqueous NaOH added dropwise as the base. FAL (1 equiv.) and 4 equiv. of epichlorohydrin (relative to FAL) were taken in a 100 mL round-bottomed flask (three-neck) equipped with a dropping funnel, an overhead mechanical stirrer, a thermometer, and an oil bath. The reaction mixture was stirred at 70 °C for 2 h. An equimolar amount of 5N aqueous NaOH solution was introduced to this reaction mixture dropwise maintaining the flow rate such that the pH of the reaction mixture was maintained at around 7.4 using a pressure-equalizing funnel (2-2.5 h). After the complete addition of NaOH solution, the reaction was continued for another 2 h at 70 °C. The reaction mixture was extracted with ethyl acetate and washed with water thrice to obtain the desired product (FAE).

#### ***Preparation of epoxy resin containing DA adducts (CYS-FGE-BMI)***

FGE (2.5 equiv.) and Cystamine (CYS) (1 equiv.) (purchased as cystamine dihydrochloride and desalinated as per the procedure by Khalafi et al. [29]) were mixed in 40 ml toluene with



mechanical stirring under N<sub>2</sub> atmosphere. The reaction was carried out at 110 °C for 20 h, during which the amino group of cystamine opened the epoxy ring of FGE. After completion of the reaction, the toluene was removed by drying under vacuum at 60 °C, and the unreacted reagents were washed with n-hexane thrice. The resulting product was cystamine-functionalized FGE (CYS-FGE).



**Scheme 4:** Plausible reaction scheme for the formation of furfuryl alcohol-based epoxy resin and the corresponding thermoset

### Curing of resin

To analyze the physical properties of the epoxy, they were converted to their thermoset form by curing with BMI. CYS-FGE to BMI mixed ratio was optimized to obtain the optimal

thermoset. Homogeneous mixtures of resins were prepared without the use of any solvent in a 25 mL beaker and cast on teflon sheets. The epoxy-coated plates were cured at a specific temperature for a specified period which was optimized by examining the swelling value of the prepared thermosets in THF. For optimal curing, this value should lie between 20 and 30%.

The swelling value of the thermosets was determined by calculating the change in weight of the thermoset after being immersed in THF solvent for 48 h. The swelling value was evaluated using the following equation-

$$\text{Swelling value (\%)} = \left[ \frac{w_s - w_d}{w_d} \right] \times 100 \quad (\text{eq. 4})$$

where  $w_s$  and  $w_d$  are the weight of the swollen and dry thermosets.

**Table 15: Optimization of curing time and curing temperature**

(CYS-FGE) : BMI	1:2	1:1.5	1:1.	1:0.5	1:0.33
<b>Temperature of curing</b>	80	80	80	90	90
<b>Time of curing</b>	12	16	24	48	60



**Figure 29: Digital images of the cured thermosets**

**Instrumentation and Methods:** As described in details of protocol of Chapter 1.

### 6.3. Results and discussion

**Structural analysis:** The physicochemical structure of the synthesized epoxy was analyzed to authenticate its proposed structure.

#### Synthesis and characterization of epoxy prepolymers

Epoxy prepolymers were prepared in a two-step synthetic procedure as depicted in Scheme 4. Glycidylation of furfuryl alcohol in an alkaline medium (pH 7.4) with excess epichlorohydrin results in the formation of furfuryl glycidyl ether (FGE). The reaction of FGE with CYS gave the corresponding epoxy prepolymer CYS-FGE. The physicochemical structure of the synthesized epoxy was analyzed to authenticate its proposed structure using FTIR,  $^1\text{H}$  NMR, and  $^{13}\text{C}$  NMR.

#### Fourier transform infrared spectroscopy (FTIR) study

Figure 30(a) shows the FTIR spectra of FGE, CYS-FGE, BMI, and CYS-FGE-BMI. The broad characteristic absorption band near  $3458\text{ cm}^{-1}$  corresponding to the OH group appears in FGE, CYS-FGE, and CYS-FGE-BMI (although FGE does not contain any OH groups, the characteristic peak might be due to the opening up of some of the epoxy groups during glycidylation). The two absorption peaks at  $2924\text{ cm}^{-1}$  and  $2859\text{ cm}^{-1}$  are assigned to aromatic and aliphatic C-H stretching, respectively. The sharp peak at  $1709\text{ cm}^{-1}$  corresponding to C=O

stretch appears for BMI, peak near  $1500\text{ cm}^{-1}$  of weak intensity corresponds to C-H bending appear in all four spectra. Peak at  $1629\text{ cm}^{-1}$  corresponds to aromatic C=C stretching. The characteristic epoxy peak at  $918\text{ cm}^{-1}$  which is assigned to C-O str. of epoxy rings in FGE is indicative of successful epoxidation which disappears in FGE-CYS due to opening up of epoxide rings by cystamine. The C-O-C stretching absorption peaks for oxirane appear at  $857\text{ cm}^{-1}$ .

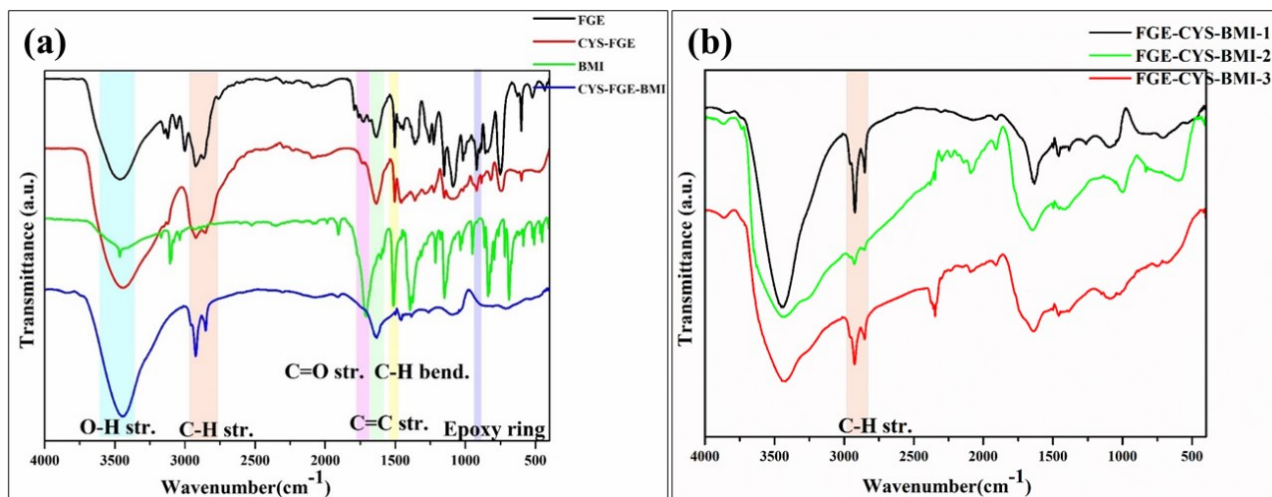


**Figure 30: (a) FTIR spectra of FGE, FGE-CYS, BMI, and FGE-CYS-BMI, (b) spectra showing comparison between the pristine thermoset FGE-CYS-BMI-80, thermoset cured at  $130^{\circ}\text{C}$  (FGE-CYS-BMI-130) and post cured at  $80^{\circ}\text{C}$  (FGE-CYS-BMI-80)**

To investigate the thermal reversibility of FGE-CYS-BMI further, FT-IR analysis was performed, with the results displayed in Figure 30(b). The peak at  $1629\text{ cm}^{-1}$  was attributed to the C=C group absorption in the maleimide ring. This peak's intensity remained almost constant throughout the heat treatment, indicating that it could serve as an internal standard for quantitative analysis. The peak at  $2924\text{ cm}^{-1}$  corresponds to the characteristic absorption of the H atom attached to the C=C bond in the maleimide ring. The intensity of this peak varied when the sample was heated between  $80\text{--}130^{\circ}\text{C}$ , suggesting the occurrence of the DA/r-DA reaction, as illustrated in Figure 30(b).

A pronounced absorption peak appeared at  $2924\text{ cm}^{-1}$  when the cracked polymer FGE-CYS-BMI-1, was cured at  $130^{\circ}\text{C}$  for 20 min, indicating the occurrence of r-DA reaction. When the thermoset was further treated at  $80^{\circ}\text{C}$  for 4 hr (FGE-CYS-BMI-2), the intensity of this absorption peak again increased on treating the thermoset at  $130^{\circ}\text{C}$  for 20 min indicating the occurrence of r-DA reaction (FGE-CYS-BMI-3), as shown in Figure 30(b).

## NMR spectral analysis

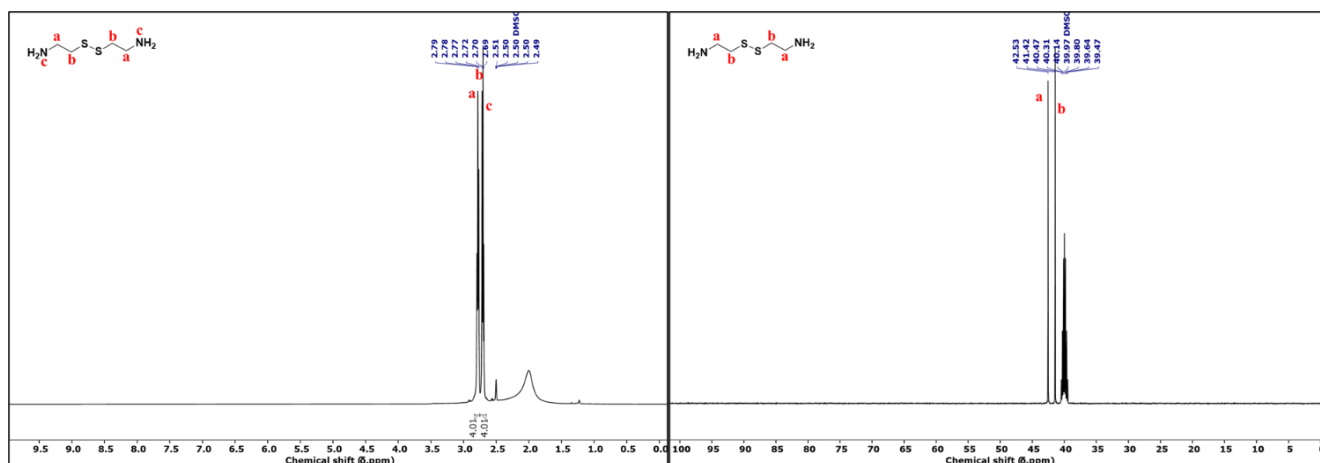


Figure 31:  $^1\text{H}$  NMR spectrum of (a) CYS and (b)  $^{13}\text{C}$  NMR spectrum of CYS

CYS:  $^1\text{H}$  NMR (500 MHz, DMSO)  $\delta$  2.78 (t,  $J = 7.4$  Hz, 4H), 2.70 (t,  $J = 6.8$  Hz, 4H).  $^{13}\text{C}$  NMR (126 MHz, DMSO)  $\delta$  42.5, 41.4.

## FGE

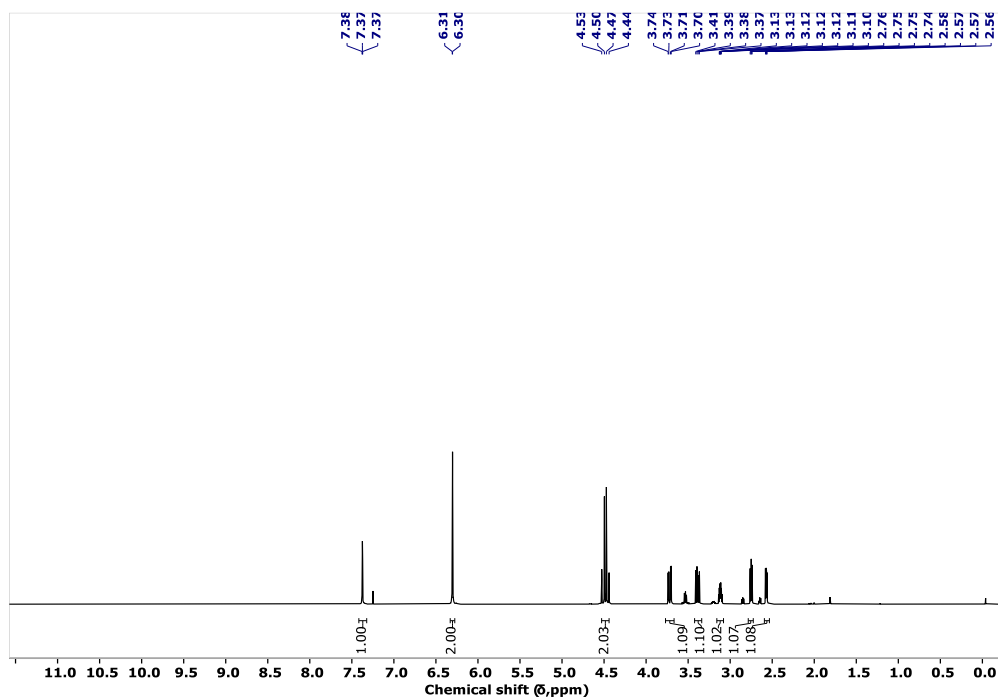


Figure 32:  $^1\text{H}$  NMR spectrum of FGE

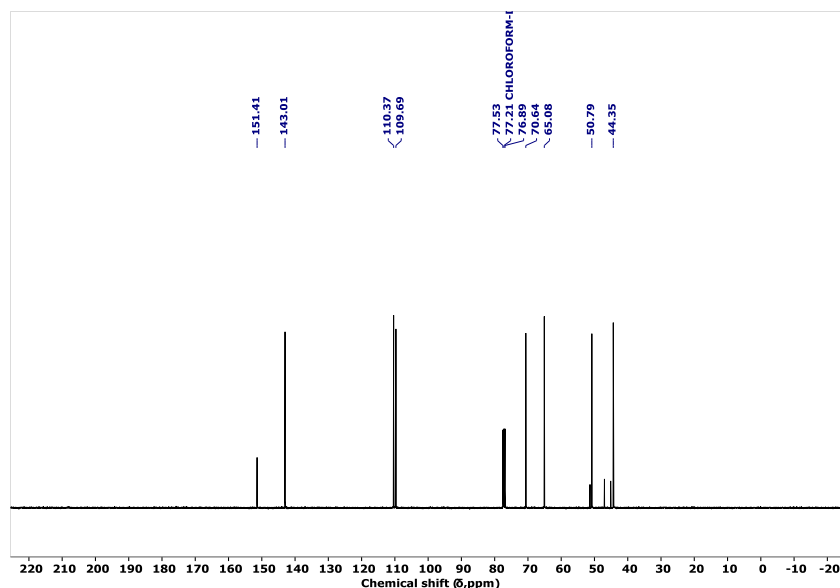


Figure 33:  $^{13}\text{C}$  NMR spectrum of FGE

**FGE:**  $^1\text{H}$  NMR (400 MHz,  $\text{CHLOROFORM-D}$ ):  $\delta$  7.37 (t,  $J = 1.4$  Hz, 1H), 6.30 (d,  $J = 1.5$  Hz, 2H), 4.53 – 4.44 (m, 2H), 3.72 (dd,  $J = 11.5, 3.1$  Hz, 1H), 3.39 (dd,  $J = 11.5, 5.9$  Hz, 1H), 3.12 (ddt,  $J = 5.8, 4.1, 2.9$  Hz, 1H), 2.75 (dd,  $J = 5.0, 4.1$  Hz, 1H), 2.57 (dd,  $J = 5.0, 2.7$  Hz, 1H).  $^{13}\text{C}$  NMR (101 MHz,  $\text{CHLOROFORM-D}$ ):  $\delta$  151.4, 143.0, 110.4, 109.7, 70.6, 65.1, 50.8, 44.3.

The  $^1\text{H}$  NMR ( $\text{CDCl}_3$ ) spectrum of FGE is shown in Figure 32. The absence of a singlet peak at around 2.5 ppm corresponding to the -OH group of FA and appearance of ddt peak at  $\delta=3.12$  ppm corresponding to the CH proton of the oxirane ring and two dd peaks at  $\delta=2.75$ , and 2.57 ppm corresponding to  $\text{CH}_2$  protons of the epoxy ring is indicative of successful epoxidation.

The  $^{13}\text{C}$  NMR ( $\text{CDCl}_3$ ) spectrum of FGE is shown in Figure 33. The peak at  $\delta=44.3$  and  $\delta=50.9$  ppm corresponding to Cs of oxirane ring is indicative of successful epoxidation.

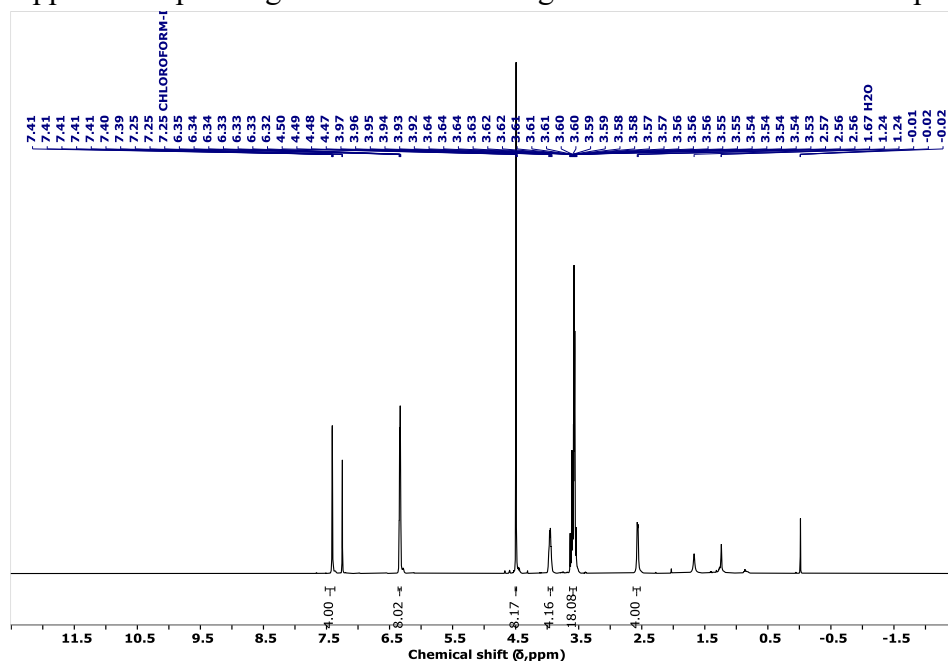


Figure 34:  $^1\text{H}$  NMR spectrum of FGE-CYS

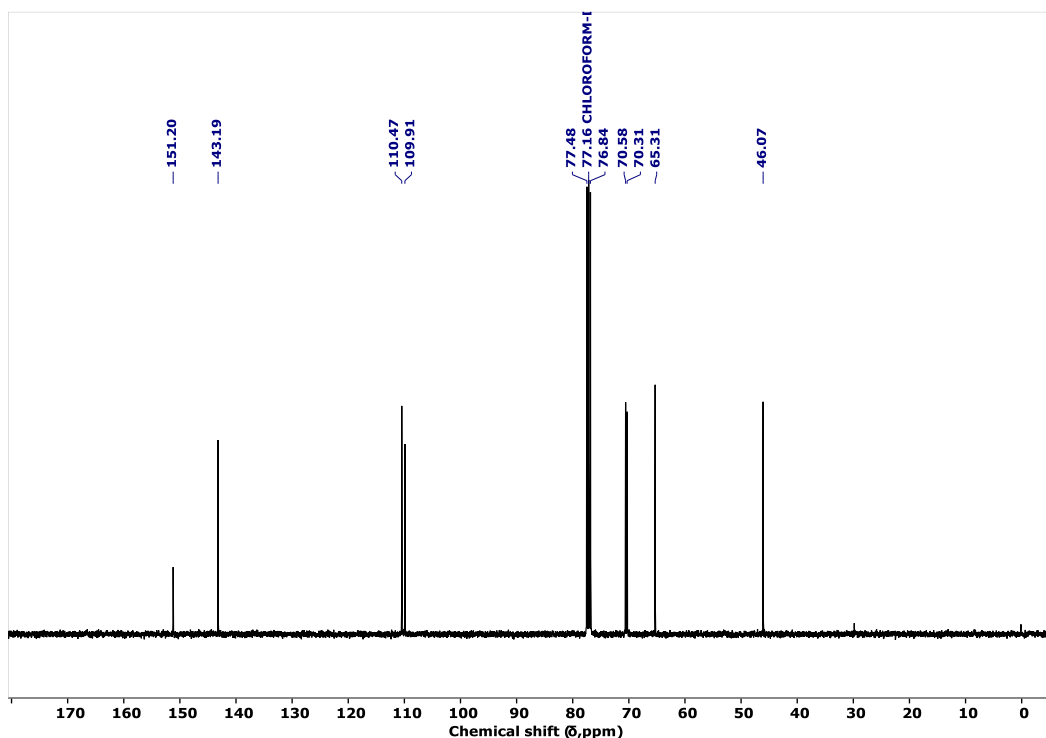


Figure 35:  $^{13}\text{C}$  NMR spectrum of FGE-CYS

**FGE-CYS:**  $^1\text{H}$  NMR (400 MHz,  $\text{CHLOROFORM-D}$ )  $\delta$  7.41 (td,  $J = 1.8, 0.9$  Hz, 4H), 6.36 – 6.32 (m, 8H), 4.50 (d,  $J = 1.7$  Hz, 8H), 3.95 (q,  $J = 5.3$  Hz, 4H), 3.64 – 3.54 (m, 18H), 2.56 (s,  $J = 5.2$  Hz, 4H).  $^{13}\text{C}$  NMR (101 MHz,  $\text{CHLOROFORM-D}$ )  $\delta$  151.2, 143.2, 110.4, 109.9, 70.6, 70.3, 65.3, 46.0.

The  $^1\text{H}$  NMR ( $\text{CDCl}_3$ ) spectrum of FGE-CYS is shown in Figure 34. The disappearance of ddt peak at  $\delta=3.12$  ppm corresponding to the CH proton of the oxirane ring and two dd peaks at  $\delta=2.75$ , and 2.57 ppm corresponding to  $\text{CH}_2$  protons of the epoxy ring and the appearance of a singlet peak at around 2.5 ppm indicates the opening up of oxirane ring by amine group of cystamine.

The  $^{13}\text{C}$  NMR ( $\text{CDCl}_3$ ) spectrum of FGE-CYS is shown in Figure 35. The disappearance of peak at  $\delta=44.3$  and  $\delta=50.9$  ppm corresponding to Cs of oxirane ring is indicative of opening up of oxirane ring.

### Thermal study of the epoxy thermosets

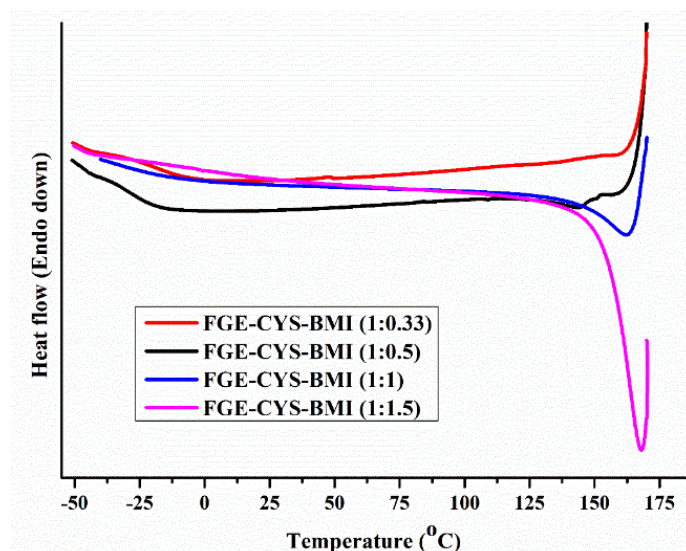


**Figure 36: DSC curves displaying glass transition temperatures for the prepared epoxy thermosets**

Thermostability is a critical property of epoxy thermosets, as it broadens the material's potential applications across various temperature ranges. FGE-CYS-BMI films were cured at 80°C, and the resulting samples were analyzed using Differential Scanning Calorimetry (DSC). The DSC measurements revealed a distinct endothermic peak between 130°C and 170°C, confirming that the r-DA reaction occurred in FGE-CYS-BMI in this temperature range.

The glass transition temperature ( $T_g$ ), an important characteristic of amorphous polymers, is influenced by several factors, including cross-linking density, the presence of polar groups, and the length of side chains. As shown in Figure 36, the DSC thermograms indicate the  $T_g$  values of the cured epoxy thermosets. It was observed that the  $T_g$  increased with a higher BMI content, which can be attributed to the formation of a denser network structure and the reduced mobility of polymer chains. This increase in cross-linking led to shorter chain lengths and a more rigid polymer structure.

**Table 16: Glass transition temperature of the thermosets**

<i>Epoxy Thermoset</i>	<i>T<sub>g</sub> (°C)</i>
<b>FGE-CYS-BMI (1:0.33)</b>	161
<b>FGE-CYS-BMI (1:0.5)</b>	162
<b>FGE-CYS-BMI (1:1)</b>	163
<b>FGE-CYS-BMI (1:1.5)</b>	168

**XRD study**

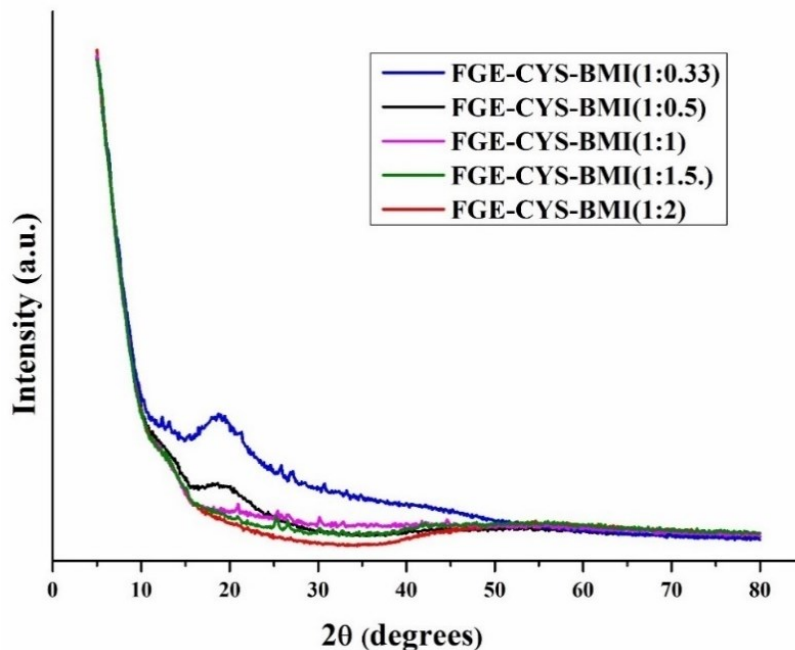


Figure 37: PXRD pattern of epoxy thermosets

X-ray diffractograms of the thermosets are shown in Figure 37, the absence of any sharp peak indicates the amorphous nature of the thermosets.

### Physical and mechanical properties

The physical properties of the epoxy thermosets were assessed and are summarized in Table 8. It was observed that the tensile strength increases with an increase in the cross-linking density between the functionalities. Figure 38 illustrates the stress-strain behaviour of a series of epoxy thermosets containing varying amounts of crosslinker. A notable reduction in tensile strength occurred as the quantity of BMI added was decreased. The higher tensile strength observed in the FGE-CYS-BMI(1:1.5) formulation can be attributed to the greater formation of DA adducts, facilitated by the higher BMI content. In contrast, as the amount of BMI per unit mass of the resin decreased from FGE-CYS-BMI (1:1.5) to CYS-FGE-BMI(1:0.33), a gradual decline in tensile strength was noted. This decrease is likely due to the reduced quantity of DA adducts per unit volume of the thermoset, leading to a lower cross-linking density.

Table 3 presents the values of several key mechanical properties of the materials, including the maximum force the material can withstand before failure (ultimate tensile strength,  $F_{\max}$  in MPa), the maximum stress the material can endure before breaking (fracture point,  $F_{\text{break}}$  in N), the change in length (dL) at the point where the maximum force ( $F_{\max}$ ) is reached (dL at  $F_{\max}$  in mm), and the change in length (dL) at the fracture point (dL at  $F_{\text{break}}$  in mm).  $L_o$  (mm) represents the original length of the sample.

A comparison of the stress-strain profiles of the pristine thermoset (subjected to 80°C) and their respective healed thermosets (cured at 130°C) revealed that the  $F_{\max}$  value of the healed samples was consistently higher than that of the pristine thermoset. Additionally, an increase in the dL at  $F_{\max}$  was observed in most cases for the healed samples.



Scratch hardness values of cured epoxy thermosets increased with the increase in cross-linking density.

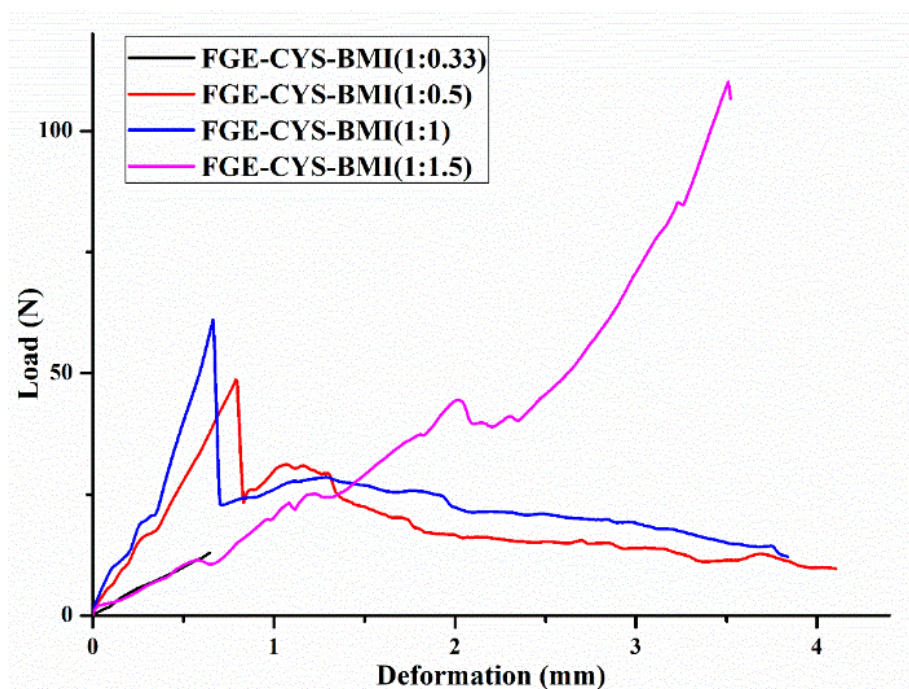


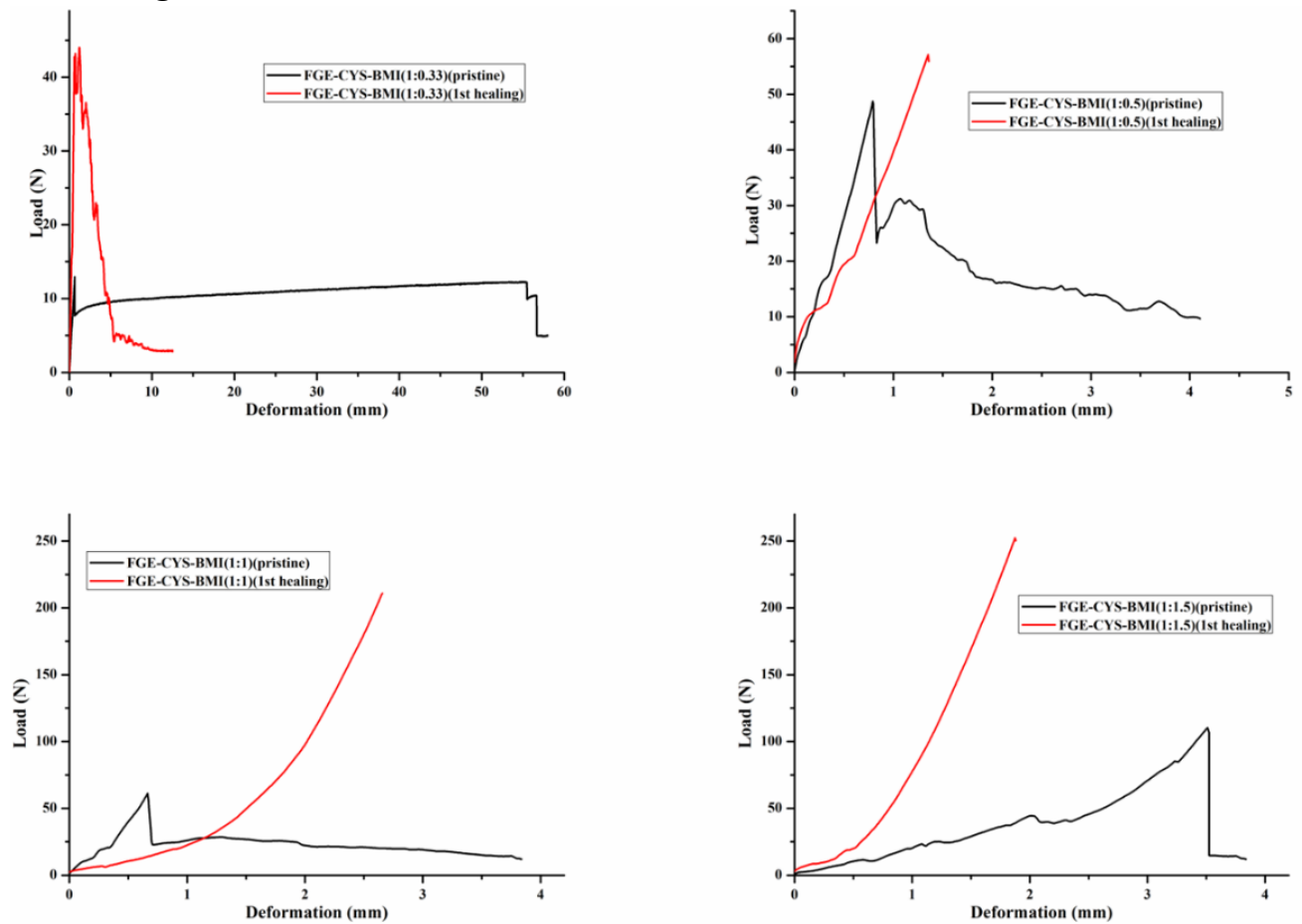
Figure 38: Stress-strain curve of pristine epoxy thermosets

Table 17: Mechanical properties of the epoxy resins along with their thermosets

Self-healing test:

Sample Code	FGE-CYS-BMI (1:0.33)	FGE-CYS-BMI (1:0.5)	FGE-CYS-BMI (1:1)	FGE-CYS-BMI (1:1.5)
Ultimate tensile strength, $F_{max}$ (MPa)	0.66	0.84	3.44	2.95
Fracture point, $F_{break}$ (N)	12.95	9.67	12.10	106.69
dL at $F_{max}$ (mm)	0.64	0.79	0.66	3.51
dL at $F_{break}$ (mm)	0.64	4.10	3.84	3.52
$L_0$ (mm)	44.69	44.69	36.69	23.69
Gloss ( $60^\circ$ )	80.2	72.86	73.19	67
Scratch resistance (kg)	3	5	5.5	7
Specific gravity of resin	1.22	1.22	1.22	1.22
Specific gravity of thermoset	1.24	1.31	1.37	1.64

## Self-healing test



**Figure 39: Stress-strain profiles of pristine along with their respective healed thermosets**

The sample was first divided into two pieces using a sharp razor blade, with the cut surfaces then placed in contact on a Teflon sheet. The sample was subsequently heated at 130°C for different durations, as detailed in Table 9, in a convection oven. To assess the healing efficiency, the percentage healing efficiency was calculated using Equation (5). Additionally, the healing process was qualitatively evaluated by capturing microscopic images of both the damaged and healed surfaces of the films using a polarizing microscope (Model: Moti BA310Pol).

The healing efficiency was determined as follows:

$$\text{Healing Efficiency (\%)} = \left( \frac{\text{Tensile strength of the healed sample}}{\text{Tensile strength of the pristine sample}} \right) \times 100 \quad (\text{eq. 5})$$

The bending strength of the material increased and even surpassed the original strength. This outcome can be attributed to the following factors: The r-DA reaction occurred at 130°C for FGE-CYS-BMI, causing the DA adducts to break, resulting in the formation of shorter molecular chains. This facilitated the movement of chains within the epoxy resin, allowing the molecules to more easily migrate and fill the gaps between the two fractured parts. As a result, the cracks were progressively repaired. However, the relatively short treatment time at 130°C did not provide sufficient molecules to fully fill the gaps, leading to incomplete repair. When the treatment time was optimized, the short molecular chains were able to completely fill the cracks, restoring the bending strength. Additionally, DA adducts were regenerated during

treatment at 80°C for 3 hours, further contributing to the recovery of the bending strength. The polymer chains became more tightly arranged than in the pristine sample due to the ease with which the shorter chains could move and migrate following the r-DA reaction. The DA reaction at 80°C enabled the regeneration of DA adducts, which played a role in restoring and even exceeding the mechanical strength of the original sample. Furthermore, prolonged treatment could result in side reactions, making it crucial to determine an optimal treatment time at 130°C for each case. In conclusion, heat treatment significantly influenced the properties of FGE-CYS-BMI.

**Table 18: Mechanical properties of the pristine along with their healed thermosets**

Sample Code	FGE-CYS-BMI (1:0.33)	FGE-CYS-BMI (1:0.5)	FGE-CYS-BMI (1:1)	FGE-CYS-BMI (1:1.5)
Duration of heat treatment at 130 °C (mins)	7	12	20	26
Ultimate tensile strength, $F_{\max}$ (MPa) of pristine thermoset	0.66	0.84	3.44	2.95
Ultimate tensile strength, $F_{\max}$ (MPa) of 1 <sup>st</sup> healed sample	1.17	1.06	4.66	11.61
dL at $F_{\max}$ (mm) of pristine thermoset	0.64	0.79	0.66	3.51
dL at $F_{\max}$ (mm) of 1 <sup>st</sup> healed sample	1.21	1.35	2.66	1.87
Healing efficiency	177%	126%	135%	393%

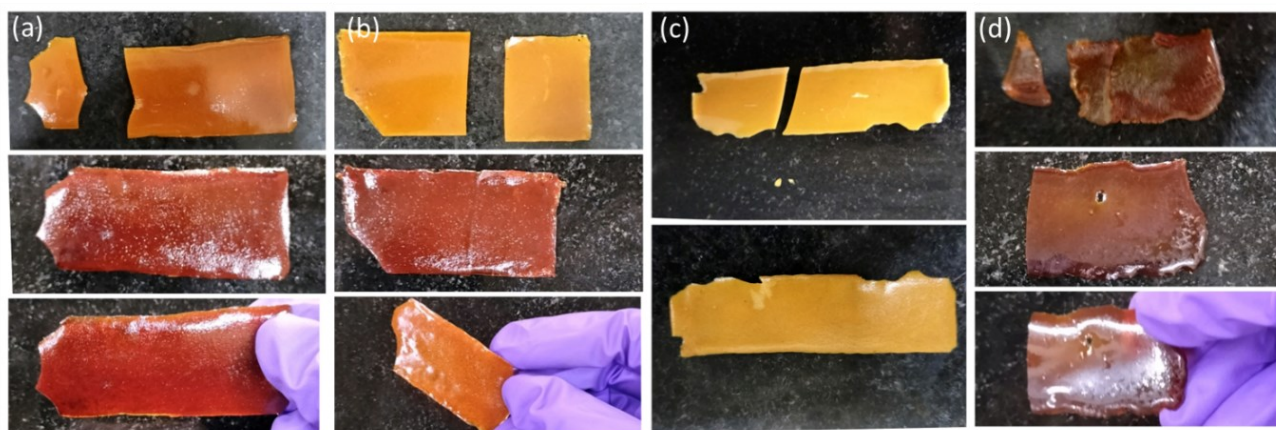


**Figure 40: Photographs of the cut and healed thermosets (a) FGE-CYS-BMI (1:1.5), (b) FGE-CYS-BMI (1:1), (c) FGE-CYS-BMI (1:0.5), (d) FGE-CYS-BMI (1:0.33)**

### Self-cleaning property

To enhance the self-cleaning properties of the prepared epoxy thermosets, we aimed to modify the surface roughness by incorporating ZnO nanoparticles. Among the various methods for

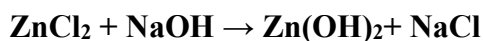
synthesizing ZnO nanoparticles (NPs) discussed in the literature, we choose the wet chemical method due to its low cost, minimal hazards, high yield, simplicity, and scalability. Chemical synthesis techniques are widely favored for these advantages.

ZnO nanoparticles, particularly at the nanoscale, are well-suited for applications requiring strong chemical stability and specific physicochemical properties, such as antibacterial activity, anti-corrosion properties, high photocatalytic performance, and ultraviolet absorption, making them ideal for use in self-cleaning coatings. Their remarkable ability to create a multiscale rough structure and exhibit chemical stability has led to considerable interest in the modification of ZnO surfaces. Researchers have explored various strategies to adjust the wettability of ZnO from hydrophilic to superhydrophobic. Superhydrophobicity can be achieved through surface modifications using materials like stearic acid, fluorinated polysiloxane, or other polymers such as polydimethylsiloxane (PDMS).

In this study, we present a simple, cost-effective approach to preparing a hydrophobic surface with a hierarchical structure, based on ZnO nanoparticles synthesized via the wet chemical method. The surface was then further modified with polydimethylsiloxane (PDMS), resulting in enhanced hydrophobicity.

### Synthesis of ZnO NPs

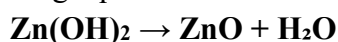
Zinc oxide nanoparticles were synthesized using a wet chemical method, with Zinc Chloride ( $\text{ZnCl}_2$ ) and Sodium Hydroxide ( $\text{NaOH}$ ) as the precursors, as represented by the following chemical equation:



To begin, 5 g of  $\text{NaOH}$  (1.0 M) was dissolved in 50 mL of distilled water. The resulting  $\text{NaOH}$  solution was then heated and stirred continuously at around  $70^\circ\text{C}$  to  $90^\circ\text{C}$ . Once the target temperature was reached, 8.5 g of  $\text{ZnCl}_2$  (0.5 M) was dissolved in 50 mL of distilled water. The  $\text{ZnCl}_2$  solution was then added dropwise into the  $\text{NaOH}$  solution leading to immediate precipitation of zinc hydroxide ( $\text{Zn(OH)}_2$ ), and the solution's color changed from transparent to white.

After completing the dropwise addition of the  $\text{ZnCl}_2$  solution, the reaction mixture was continuously stirred for two hours while maintaining the desired temperature. Following this, zinc hydroxide, along with some unknown impurities, settled at the bottom of the container, and the excess mother liquor was carefully removed to remove the dissolved  $\text{NaCl}$ . The resulting precipitate was centrifuged for 10 minutes. The precipitate was then washed five times with deionized water and methanol to remove any residual by-products bound to the zinc hydroxide.

Finally, the washed precipitate was dried in an air atmosphere at approximately  $400^\circ\text{C}$ . This drying process resulted in the complete conversion of zinc hydroxide ( $\text{Zn(OH)}_2$ ) into zinc oxide ( $\text{ZnO}$ ), as represented by the following equation:



This method results in the formation of ZnO nanoparticles, which can be further characterized and analyzed for their properties.

#### **Functionalisation of ZnO NPs with PDMS:**

First, 0.2 g of zinc oxide nanoparticles were dispersed in 10 ml of toluene and ultrasonicated for 15 minutes. To this dispersion, 1 ml of 10% polydimethylsiloxane (PDMS) and 0.1 ml of 5% dibutyltin dilaurate (DBT) were added. The mixture was continuously stirred using a magnetic stirrer for 40 minutes. During the reaction of FGE with CYS, after the completion of the reaction, 5 wt% and 10 wt% ZnO in toluene were added to the stirring mixture, and the reaction continued for 30 more minutes. Once the reaction was finished, the toluene was removed by drying the mixture under vacuum at 60 °C. The resulting product was then cross-linked with BMI to obtain the nanocomposites FGE-CYS-BMI-Z(5%) and FGE-CYS-BMI-Z(10%).

#### **Characterization of the synthesized ZnO NPs**

ZnO NPs were characterized using FTIR, SEM, PXRD, UV-visible spectroscopy.

##### **UV visible spectroscopy**

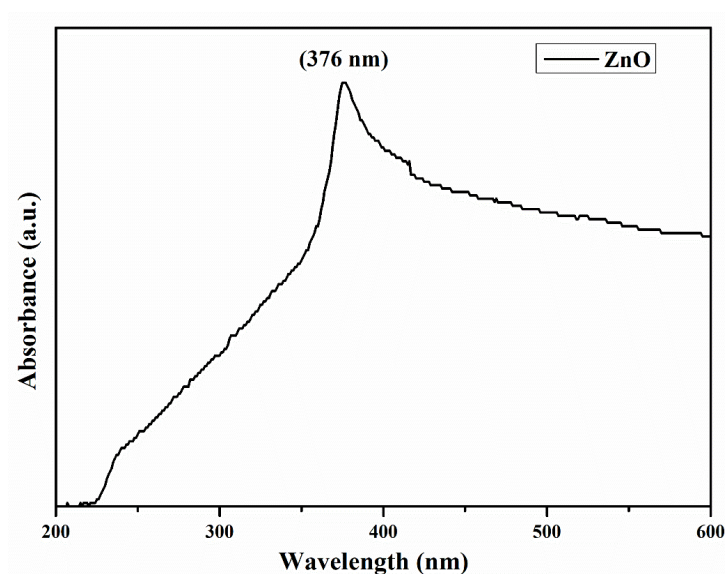


**Figure 41: UV-visible absorption spectra of ZnO nanoparticles**

The UV–visible absorption spectrum of the ZnO nanoparticles is shown in Figure 41, recorded at room temperature within the wavelength range of 200–600 nm. The spectrum exhibits a prominent peak at 376 nm, which corresponds to a wide band gap of 3.37 eV.

#### **FTIR study of the synthesized nanoparticles along with their nanocomposites:**

FTIR analysis was performed to identify the composition and ensure the efficient stabilization of the synthesized ZnO nanoparticles (ZnO NPs).



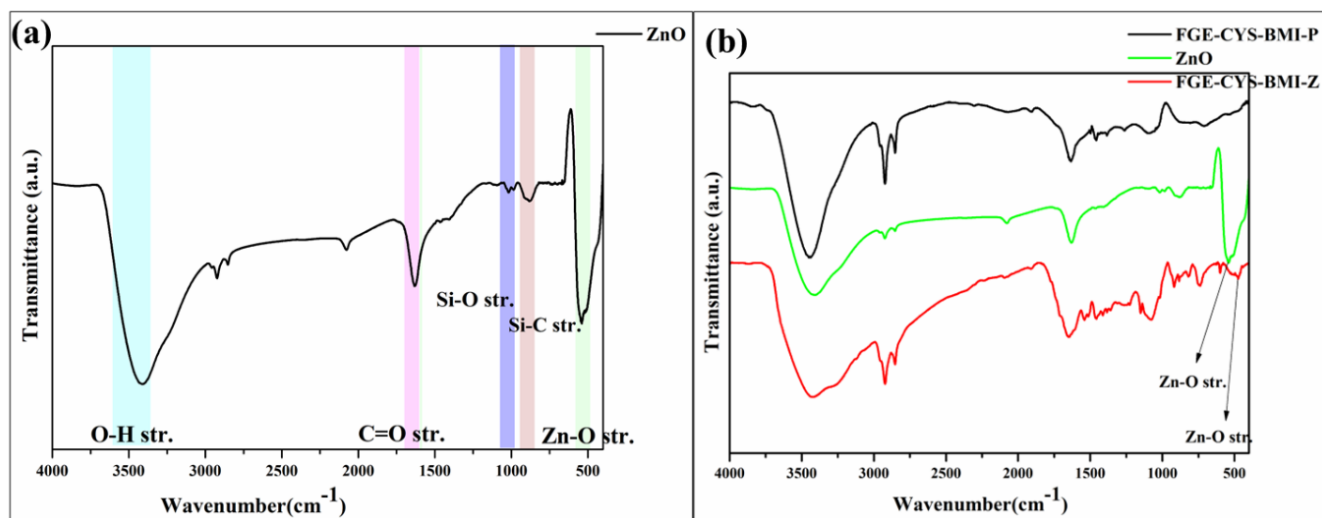


**Figure 42: FTIR spectra of (a) ZnO NPs, (b) Spectra of ZnO NPs along with the nanocomposite, and the pristine thermoset**

The FTIR spectrum of the synthesized ZnO nanoparticles (ZnO NPs) shows a strong absorption band at  $539\text{ cm}^{-1}$ , which is attributed to the stretching vibration of Zn-O. A characteristic band at  $1628\text{ cm}^{-1}$  corresponds to the stretching vibration mode of C=O residues, likely due to atmospheric  $\text{CO}_2$ . Additionally, the peak at  $3406\text{ cm}^{-1}$  is assigned to the O-H bending vibration of physisorbed water. These FTIR results confirm the successful preparation of the ZnO NPs for further evaluation in this study. The presence of Si-O and Si-C peaks at  $1012\text{ cm}^{-1}$  and  $892\text{ cm}^{-1}$  respectively indicates the functionalization of ZnO NPs.

The occurrence of an absorption peak at  $469\text{ cm}^{-1}$  in FGE-CYS-BMI-Z (Figure 42(b)) which was initially absent in the pristine polymer (FGE-CYS-BMI-P) indicates the incorporation of the ZnO nanoparticle in the nanocomposite. The Zn-O vibrational peak at  $\text{cm}^{-1}$  shifted from  $540\text{ cm}^{-1}$  in ZnO to  $469\text{ cm}^{-1}$  indicating the interaction of the functional groups of the pristine polymer with functionalized ZnO.

#### PXRD

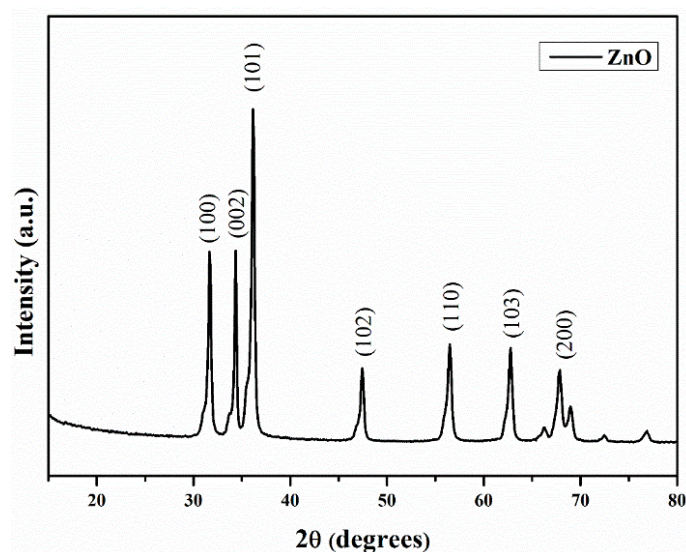


**Figure 43: PXRD pattern of synthesized ZnO NPs**

The X-ray diffraction (XRD) pattern of the synthesized ZnO nanoparticles (ZnO NPs) is shown in Figure 43. The diffraction peaks observed at  $2\theta$  values of  $31.68^\circ$ ,  $34.36^\circ$ ,  $36.16^\circ$ ,  $47.48^\circ$ ,  $56.47^\circ$ ,  $62.83^\circ$ , and  $67.83^\circ$  correspond to the Miller planes (100), (002), (101), (102), (110), (103), and (200), which are characteristic of the hexagonal wurtzite structure of ZnO. These peaks indicate that the synthesized ZnO nanoparticles exhibit excellent crystalline quality and a well-controlled morphology. The crystallite size (D) of the ZnO nanoparticles was calculated using the Scherrer equation:

$$D = K\lambda / (\beta \cos\theta)$$

Where:

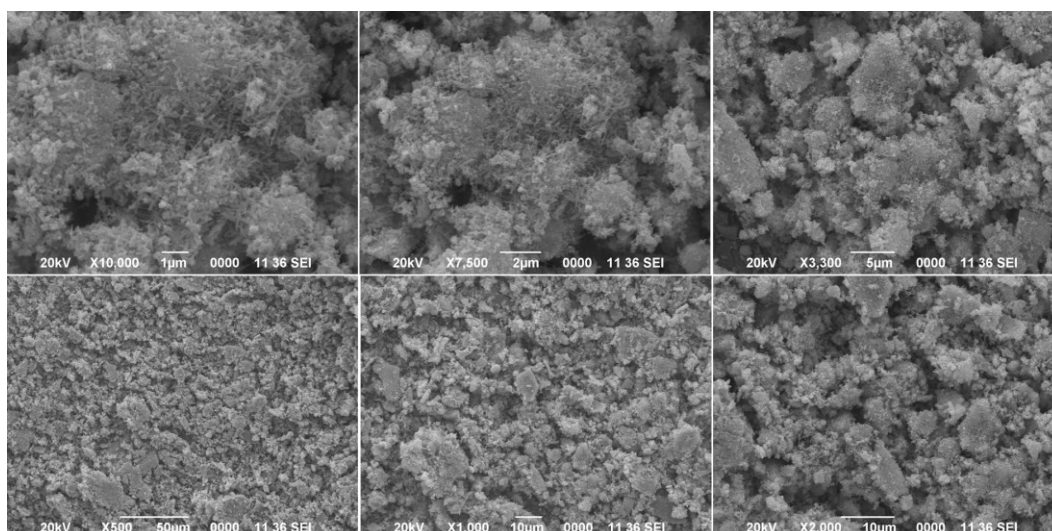
- D is the crystallite size,
- K is the shape factor which is usually taken as about 0.94,
- $\lambda$  is the X-ray wavelength used ( $1.5406 \text{ \AA}$ ),
- $\beta$  is the full width of half maximum , and
- $\theta$  is the diffraction angle.

<b><math>2\theta</math> (in degrees)</b>	31.65	34.35	36.17	47.48	56.47	62.83	67.83
<b>Crystallite size</b>	26.94	31.01	23.58	20.59	18.83	19.43	15.38

Based on this analysis, the average crystallite size of the ZnO nanoparticles was determined to be between 15 nm and 31 nm. This further confirms the high crystalline quality and nanometer-scale size of the synthesized ZnO nanoparticles.

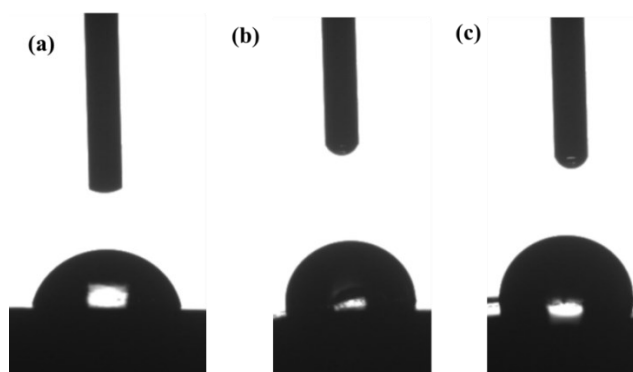
## SEM

Figure 44 shows the FESEM images of unmodified ZnO nanoparticles, which reveal varying particle sizes, their distribution, and changes in morphology. The morphology of the ZnO nanoparticles was analyzed using scanning electron microscopy at three different resolutions. The analysis confirms the presence of nanoparticles with a mixed morphology, including nanoflower, nanorod, and nanoflake-like structures.



**Figure 44: SEM images of ZnO particles showing their morphology at different resolutions**

#### **Contact angle (CA) measurement:**



**Figure 45: CA measurements of (a) FGE-CYS-BMI(1:1), (b) FGE-CYS-BMI-Z(5%) and (c) FGE-CYS-BMI-Z(10%)**

Self-cleaning performance is a key property of superhydrophobic coatings for practical applications, and it is influenced by both surface structure and chemical composition. To investigate the self-cleaning property Sessile drop method was employed with a droplet size of 2  $\mu$ l. The CA of the pristine epoxy thermoset FGE-CYS-BMI(1:1) was  $78 \pm 3.5^\circ$ , indicating its hydrophilic nature. When the epoxy was mixed with functionalized ZnO nanoparticles, the CA increased to  $100.0 \pm 2.8^\circ$  and  $98 \pm 0.5^\circ$  for FGE-CYS-BMI-Z(10%) and FGE-CYS-BMI-Z(5%) respectively. This increase in CA demonstrates that the coating becomes more hydrophobic compared to the pristine one, thereby enhancing the self-cleaning performance of the thermoset.

#### **Self-cleaning test:**



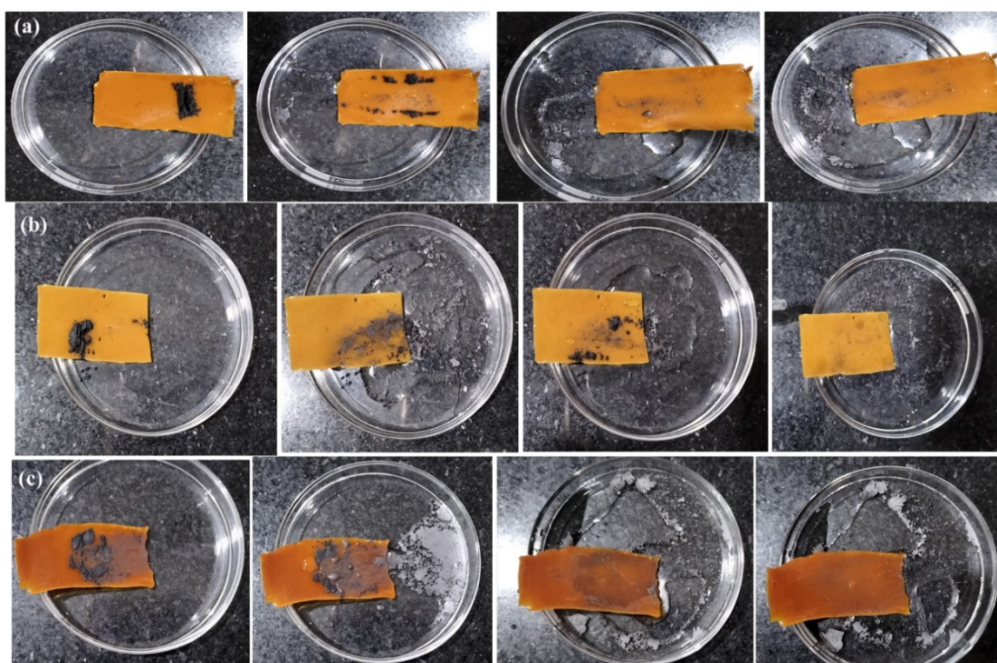


**Figure 46: Self-cleaning test of (a) FGE-CYS-BMI(1:1), (b) FGE-CYS-BMI-Z(5%) and (c) FGE-CYS-BMI-Z(10%)**

Artificial dirt was first sprayed on the coatings. The contaminated samples were then mounted on at a slanted angle of 45 °C before being cleaned with water spray using a fixed volume of 5 mL. It was observed that excellent cleaning was observed in case of the nanocomposite films which was not observed in case of pristine thermoset as depicted in figure 46.

## 1. Traceability Matrix: Objectives and Work done

Objectives	Workdone-1	Workdone-2	Workdone-3	Workdone-4
Objective-1	√	√	√	√
Objective-2				√
Objective-3				√
Objective-4	√	√	√	√
Objective-5				√
Objective-6				√
Objective-7				√

## 2. Feedback from Lab/ Domain Scientist

## 3. Traceability Matrix: Milestone Reports and Work done

Objectives	Workdone-1	Workdone-2	Workdone-3	Workdone-4
Milestone Report-1	√	√		
Milestone Report-2			√	
Milestone Report-3				√

## 4. Traceability Matrix: Publications and Work done

Objectives	Workdone-1	Workdone-2	Workdone-3	Workdone-4
Publication-1 (Journal)			√	
Publication-2 (Journal)				
Publication-3 (Journal)				√
Publication-4 (Conference)			√	

## 11. Future Work: Extensions and Exploitation

1. While the brittleness of thermosets has been addressed by varying the bismaleimide content, further optimization of their physical properties can be achieved by employing chain extension techniques with bismaleimide. This approach could enhance both the mechanical properties and optimize the flexibility of the thermoset.
2. Efforts to improve the tensile properties of thermosets have focused on varying the amount of crosslinking agents. Future work could investigate the incorporation of different types of crosslinkers and diamine chain extenders to further enhance the mechanical strength and long-term durability of the thermosets.
3. ZnO nanoparticles have been functionalized to improve the hydrophobicity of thermosets. Future research could explore the use of various functional groups on ZnO nanoparticles to optimize their contact angle and further improve the water resistance of the composites.
4. The photocatalytic properties of ZnO nanoparticle-incorporated thermosets remain underexplored. Future studies could focus on a more detailed evaluation of these materials under different light conditions to maximize their photocatalytic efficiency, particularly for applications in self-cleaning.
5. Initial efforts have been made to incorporate ZnO nanoparticles into thermosets for self-cleaning applications. Further investigations could explore a wider range of nanoparticles and their interactions with the thermoset matrix, which may lead to the development of more efficient self-cleaning thermosets with enhanced performance under varying environmental conditions.
6. Thermosets can be further modified to incorporate advanced smart properties, such as shape memory and reprocessability. Investigating these functionalities could open up new applications in adaptive materials and recyclable composites, enhancing their versatility and sustainability.

## References

- [1] Jin, F. L., Li, X., & Park, S. J. (2015). Synthesis and application of epoxy resins: A review. *Journal of Industrial and Engineering Chemistry*, 29, 1-11.
- [2] Baroncini, E. A., Kumar Yadav, S., Palmese, G. R., & Stanzione III, J. F. (2016). Recent advances in bio-based epoxy resins and bio-based epoxy curing agents. *Journal of Applied Polymer Science*, 133(45).

- [3] Epoxy Adhesives Market Size, Share & Trends Analysis Report By Application (Automotive & Transportation, Building & Construction), By Technology, By Region, And Segment Forecasts, 2021 – 2028
- [4] Ma, S., Liu, X., Fan, L., Jiang, Y., Cao, L., Tang, Z., & Zhu, J. (2014). Synthesis and properties of a Bio-Based epoxy resin with high epoxy value and low viscosity. *ChemSusChem*, 7(2), 555-562.
- [5] Flint, S., Markle, T., Thompson, S., & Wallace, E. (2012). Bisphenol A exposure, effects, and policy: a wildlife perspective. *Journal of environmental management*, 104, 19-34.
- [6] Vom Saal, F. S., & Hughes, C. (2005). An extensive new literature concerning the low-dose effects of bisphenol A shows the need for a new risk assessment. *Environmental health perspectives*, 113(8), 926-933.
- [7] Fulcrand, H., Rouméas, L., Billerach, G., Aouf, C., & Dubreucq, E. (2019). Advances in bio-based thermosetting polymers. *Recent Advances in Polyphenol Research*, 6, 285-334.
- [8] Czub, P. (2009). Synthesis of high-molecular-weight epoxy resins from modified natural oils and Bisphenol A or BisphenolA-based epoxy resins. *Polymers for Advanced Technologies*, 20(3), 194-208.
- [9] Jailliet, F., Darroman, E., Ratsimihety, A., Auvergne, R., Boutevin, B., & Caillol, S. (2014). New biobased epoxy materials from cardanol. *European Journal of Lipid Science and Technology*, 116(1), 63-73.
- [10] El Mansouri, N. E., Yuan, Q., & Huang, F. (2011). Synthesis and characterization of kraft lignin-based epoxy resins. © *BioResources*, 2011, vol. 6, núm. 3, p. 2492-2503.
- [11] El Mansouri, N. E., Yuan, Q., & Huang, F. (2011). Synthesis and characterization of kraft lignin-based epoxy resins. © *BioResources*, 2011, vol. 6, núm. 3, p. 2492-2503.
- [12] Łukaszczyk, J., Janicki, B., & Kaczmarek, M. (2011). Synthesis and properties of isosorbide-based epoxy resin. *European Polymer Journal*, 47(8), 1601-1606.
- [13] Koike, T. (2012). Progress in the development of epoxy resin systems based on wood biomass in Japan. *Polymer Engineering & Science*, 52(4), 701-717.
- [14] Shibata, M., & Nakai, K. (2010). Preparation and properties of biocomposites composed of bio-based epoxy resin, tannic acid, and microfibrillated cellulose. *Journal of Polymer Science Part B: Polymer Physics*, 48(4), 425-433.
- [15] Kiattipornpithak, K., Thajai, N., Kanthiya, T., Rachtanapun, P., Leksawasdi, N., Phimolsiripol, Y., ... & Jantanasakulwong, K. (2021). Reaction mechanism and mechanical property improvement of poly (lactic acid) reactive blending with epoxy resin. *Polymers*, 13(15), 2429.
- [16] Niedermann, P., Szebényi, G., & Toldy, A. (2015). Characterization of high glass transition temperature sugar-based epoxy resin composites with jute and carbon fibre reinforcement. *Composites Science and Technology*, 117, 62-68.

- [17] Arthur, D. E., Jonathan, A., Ameh, P. O., & Anya, C. (2013). A review on the assessment of polymeric materials used as corrosion inhibitor of metals and alloys. *International Journal of Industrial Chemistry*, 4(1), 1-9.
- [18] Lenz, D. M., Delamar, M., & Ferreira, C. A. (2003). Application of polypyrrole/TiO<sub>2</sub> composite films as corrosion protection of mild steel. *Journal of Electroanalytical Chemistry*, 540, 35-44.
- [19] Timmerman, J. F., Hayes, B. S., & Seferis, J. C. (2003). Cryogenic microcracking of carbon fiber/epoxy composites: influences of fiber-matrix adhesion. *Journal of composite materials*, 37(21), 1939-1950.
- [20] Xu, Y., & Chen, D. (2016). A novel self-healing polyurethane based on disulfide bonds. *Macromolecular Chemistry and Physics*, 217(10), 1191-1196.
- [21] An, H., Bo, Y., Chen, D., Wang, Y., Wang, H., He, Y., & Qin, J. (2020). Cellulose-based self-healing hydrogel through boronic ester bonds with excellent biocompatibility and conductivity. *RSC advances*, 10(19), 11300-11310.
- [22] Ying, H., Zhang, Y., & Cheng, J. (2014). Dynamic urea bond for the design of reversible and self-healing polymers. *Nature communications*, 5(1), 1-9.
- [23] Liu, J. D., Du, X. Y., Wang, C. F., Li, Q., & Chen, S. (2020). Construction of triple non-covalent interaction-based ultra-strong self-healing polymeric gels via frontal polymerization. *Journal of Materials Chemistry C*, 8(40), 14083-14091.
- [24] Duarah, R., & Karak, N. (2018). High performing smart hyperbranched polyurethane nanocomposites with efficient self-healing, self-cleaning and photocatalytic attributes. *New Journal of Chemistry*, 42(3), 2167-2179.
- [25] Canadell, J., Goossens, H., & Klumperman, B. (2011). Self-healing materials based on disulfide links. *Macromolecules*, 44(8), 2536-2541.
- [26] Chowdhury, R. A., Hosur, M. V., Nuruddin, M., Tcherbi-Narteh, A., Kumar, A., Boddu, V., & Jeelani, S. (2015). Self-healing epoxy composites: preparation, characterization and healing performance. *Journal of materials research and technology*, 4(1), 33-43.
- [27] Hia, I. L., Chan, E. S., Chai, S. P., & Pasbakhsh, P. (2018). A novel repeated self-healing epoxy composite with alginate multicore microcapsules. *Journal of Materials Chemistry A*, 6(18), 8470-8478.
- [28] Zhang, C., Wang, X., Liang, D., Deng, H., Lin, Z., Feng, P., & Wang, Q. (2021). Rapid self-healing, multiple recyclability and mechanically robust plant oil-based epoxy resins enabled by incorporating tri-dynamic covalent bonding. *Journal of Materials Chemistry A*, 9(34), 18431-18439.
- [29] Khalafi, H. R., Ehsani, M., & Khonakdar, H. A. (2021). Investigation of the cure kinetics and thermal stability of an epoxy system containing cystamine as curing agent. *Polymers for Advanced Technologies*, 32(3), 1251-1261.

**Minutes of Closure Project Review Committee (PRC) Meeting**

1. Closure Project Review Committee (PRC) meeting of Dte of ER&IPR sponsored Grants-in-Aid project titled “**Self-Healing and Self-Cleaning Epoxy Thermosetting Nanocomposites**” was held on **20<sup>th</sup> March, 2025 (10:00 hrs)** through Video Conference.
2. The following members have attended the meeting:-
 

Dr A B Samui, Sc-G (Retd.), NMRL, DRDO	: Chairperson
Sh S P Mishra, Assoc. Director, Dte of ER&IPR	: Member
Dr Debdatta Ratna, Sc-G, NMRL, DRDO	: Member
Dr P Sivaraman, Sc-F, NMRL, DRDO	: Member
Sh Rahul Yadav, Sc-B, NMRL, DRDO	: Member
Dr M K Pandey, Addl. Director, Dte of ER&IPR	: Member
Sh Abhisar Hudda, Dte of ER&IPR	: Member
Dr Sajal Kumar Das, Tezpur University (PI)	: Member
Ms Kirti Yadav, Tezpur University	: In-attendance
3. Sh S P Mishra welcomed the Chairperson and all members of the PRC. He briefed about the overall objectives of the project and requested the Chairperson to give his opening remarks.
4. Dr A B Samui, Chairperson in his opening remarks highlighted the importance of the project objectives and suggested this project deliverables will be useful to NMRL (DRDO). He requested the PI to present the work carried out in the project titled “Self-Healing and Self-Cleaning Epoxy Thermosetting Nanocomposites”.
5. Dr Sajal K Das, PI presented the status of project objectives and deliverables as follows:

<b>Project Objectives</b>	<b>Status of Project Objectives</b>
To develop a hyperbranched epoxy thermosetting nanocomposite as a self-healing material with self-cleaning attribute.	Achieved
<b>Project Deliverables</b>	<b>Status of Project Deliverables</b>
Self-healing and self-cleaning thermosetting materials	Completed
Technique to achieve smart epoxy materials	Completed
High performance, heavy duty epoxy coating for marine application	Completed

PI presented progress of project as compared with activity-time chart, recommendation of previous review meeting and action taken by project team, major breakthroughs, potential applications, national and international status, methodology, experimental details and results etc. PI presented the research publications/ oral presentations in the project, infrastructure developed, and manpower trained. The PI also stated that the detailed technical completion report has been submitted to NMRL (DRDO).

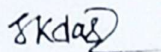
Lastly, the PI presented financial status of the project.

**6. Recommendations:**

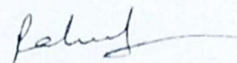
The committee was satisfied with the work carried out in the project and made the following recommendations:

- i. The PI needs to compile detailed characterization reports wrt developed material and re-submit the technical completion report to DRDO for their feedback within 15 days.

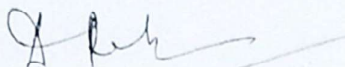
- ii. **The committee noted that the objectives and deliverables of the project have been mostly met and recommended the closure of project.** PI needs to submit the audited financial and technical documents required for the closure of project within a month to Dte of ER&IPR for processing the case for closure.




(Dr. Sajal Kumar Das)  
PI, Tezpur University



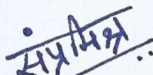
(Sh. Rahul Yadav)  
Sc-III, NMRL



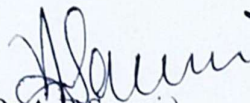
(Dr. Debdatta Ratna)  
Sc-G, NMRL



(Dr. MK Pandey)  
Dte of ER&IPR



(S. P. Mishra)  
Assoc. Director, Dte of ER&IPR



(Dr. A. B. Samui)  
Chairperson, PRC



## Consolidated Statement of Expenditure Accounts

Submitted for period (17/12/2021 to 16/12/2024)

- (a) Title of the Project: **Self-healing and self-cleaning epoxy thermosetting nanocomposites**
- (b) Sanctioned letter no. & date: **ERIP/ER/202103001/M/01/1785, dated 10 May 2021**
- (c) Principal Investigator: **Dr. Sajal Kumar Das**
- (d) Date of Start of the Project: **17/12/21**
- (e) Total Sanctioned cost of the Project: in Rs. : **Rs. 28.85 lakhs**
- (f) Grant received (Rs.) in I<sup>st</sup> yr : **Rs 9,42,000/-**      II<sup>nd</sup> yr: **Rs 8,56,472/-**      III<sup>rd</sup> yr: **Rs 9,06,965/-**
- (g) Total Grants received so far: **Rs 27,05,437/-**

S. No.	Sanctioned Heads	Funds Sanctioned	Funds released by DRDO (Financial Year wise)			Funds returned to DRDO	Total funds available during the period 17/12/2021 to 16/12/2024 (4+5+6)	Expenditure (Financial Year wise)				Balance 8-12
			1 <sup>st</sup> year during period from 17/12/21 to 31/3/22 and 1/4/22 31/3/23	2 <sup>nd</sup> year during period from 1/4/23 to 31/3/24	3 <sup>rd</sup> year during period from 1/4/24 to 16/12/24			1 <sup>st</sup> year during period from 17/12/21 to 31/3/22 and 1/4/22 31/3/23	2 <sup>nd</sup> year during period from 1/4/23 to 31/3/24	3 <sup>rd</sup> year during period from 1/4/24 to 16/12/24	Total (9+10+11)	
1	2	3	4	5	6	7	8	9	10	11	12	13
(a)	Staff	13,51,000/-	4,32,000/-	3,50,920/-	4,27,000/-	Nil	12,09,920/-	3,50,920/-	3,72,000/-	2,94,065/-	10,16,985/-	1,92,935/-
(b)	Equipment	Nil	Nil	Nil	Nil	Nil	Nil	Nil	Nil	Nil	Nil	Nil

SKDas  
29.01.25



(c)	Operation & Maintenance	3,00,000/-	1,00,000/-	1,00,000/-	98,607/-	Nil	2,98,607/-	1,00,000/-	98,607/-	97,699/-	2,96,306/-	2,301/-
(d)	Expendables	5,40,000/-	1,80,000/-	1,79,149/-	1,70,854/-	Nil	5,30,003/-	1,79,149/-	1,70,854/-	1,79,685/-	5,29,688/-	315/-
(e)	Travel	1,50,000/-	50,000/-	46,772/-	32,095/-	Nil	1,28,867/-	46,772/-	32,095/-	31,967/-	1,10,834/-	18,033/-
(f)	Contingencies	1,50,000/-	50,000/-	49,631/-	49,907/-	Nil	1,49,538/-	49,631/-	49,907/-	48,116/-	1,47,654/-	1,884/-
(g)	Visiting Faculty	Nil	Nil	Nil	Nil	Nil	Nil	Nil	Nil	Nil	Nil	Nil
(h)	Procured Service	3,00,000/-	1,00,000/-	1,00,000/-	94,502/-	Nil	2,94,502/-	1,00,000/-	94,502/-	1,00,000/-	2,94,502/-	Nil
(i)	Overhead	94,000/-	30,000/-	30,000/-	34,000/-	Nil	94,000/-	30,000/-	30,000/-	34,000/-	94,000/-	Nil
(j)	Interest earned, if any	-	9,856/-	2,632/-	4,037/-	12,488/-	16,525/-	Nil	9,856/-	2,632/-	12,488/-	4,037/-
	TOTAL	28,85,000/-	9,51,856/-	8,59,104/-	9,11,002/-	12,488/-	27,21,962/-	8,56,472/-	8,57,821/-	7,88,164/-	25,02,457/-	2,19,505/-

Signature of Principal Investigator

**Dr. Sajal Kumar Das**  
Assistant Professor  
Dept. of Chemical Sciences  
Tezpur University

Signature of Administrative Authority of  
Institute with seal

**Registrar**  
**Tezpur University**



**AUDITED STATEMENT OF EXPENDITURE ACCOUNTS**  
FOR THE FINANCIAL YEAR: 2024-25 (01/04/24 to 16/12/24)

- (a) Title of the Project: **Self-healing and self-cleaning epoxy thermosetting nanocomposites**  
 (b) Sanctioned letter no. & date: **ERIP/ER/202103001/M/01/1785, dated 10 May 2021**  
 (c) Principal Investigator : **Dr. Sajal Kumar Das**  
 (d) Date of Start of the Project: **17/12/21**  
 (e) Total Sanctioned cost of the Project : Rs. 28.85 lakhs  
 (f) Grant received (Rs.) in I yr: **Rs 9,42,000/-** II yr: **Rs 8,56,472/-** III yr: **Rs 9,06,965/-**  
 (g) Total Grants received so far: **Rs 27,05,437/-**

S. No.	Sanctioned Heads	Funds sanctioned for FY 2024-25 (Rs)	Funds released for FY 2024-25 (Rs.)	Carried forward from FY 2023-24 (Rs)	Funds available for FY 2024-25 (iv+v) (Rs)	Expenditure incurred during the FY 2024-25 (Rs)	Balance (vi-vii) Rs.	Commitments Rs.	Total expenditure (vii+ix) Rs.
i	ii	iii	iv	v	vi	vii	viii	ix	x
(a)	Staff	4,87,000/-	4,27,000/-	60,000/-	4,87,000/-	2,94,065.00/-	1,92,935/-	Nil	2,94,065.00/-
(b)	Equipment	Nil	Nil	Nil	Nil	Nil	Nil	Nil	Nil
(c)	Operation & Maintenance	1,00,000/-	98,607/-	1,393/-	1,00,000/-	97,699/-	2,301/-	Nil	97,699/-
(d)	Expendables	1,80,000/-	1,70,854/-	9,146/-	1,80,000/-	1,79,685/-	315/-	Nil	1,79,685/-
(e)	Travel	50,000/-	32,095/-	17,905/-	50,000/-	31,967/-	18,033/-	Nil	31,967/-
(f)	Contingencies	50,000/-	49,907/-	93/-	50,000/-	48,116/-	1,884/-	Nil	48,116/-
(g)	Research Consultant	Nil	Nil	Nil	Nil	Nil	Nil	Nil	Nil
(h)	Procured Service	1,00,000/-	94,502/-	5,498/-	1,00,000/-	1,00,000/-	Nil	Nil	1,00,000/-
(i)	Institutional over head	34,000/-	34,000/-	Nil	34,000/-	34,000/-	Nil	Nil	34,000/-
(j)	Interest earned, if any	Nil	4,037/-	2,632/-	6,669/-	2,632/-*	4,037/-	Nil	2,632/-
	<b>TOTAL</b>	10,01,000/-	9,11,002/-	96,667/-	10,07,669/-	7,88,164/-	2,19,505/-	Nil	7,88,164/-

\*This is the Bank Interest amount (for previous FY 2023-24) that was returned to DRDO in FY 2024-25 via Demand Draft

Name and Signature of Principal Investigator  
Date: 29.1.25

**Dr. Sajal Kumar Das**  
Assistant Professor  
Dept. of Chemical Sciences,  
Tezpur University

Name and Signature of Accounts Officer  
Date:

**Finance Officer**  
**Tezpur University**

Signature of Administrative  
Date:

**Registrar**  
**Tezpur University**



**AUDITED UTILIZATION CERTIFICATE**  
**FOR THE FINANCIAL YEAR 2024-2025 (From 01/04/24 to 16/12/24)**

1.	Title of the Project / Scheme	Self-healing and self-cleaning epoxy thermosetting nanocomposites																						
2.	Name of the Institution	Tezpur University																						
3.	Principal Investigator	Dr. Sajal Kumar Das																						
4.	DRDO Letter No. and date of sanctioning the project  Date of Start of the Project	ERIP/ER/202103001/M/01/1785, dated 10 May 2021  17/12/21																						
5.	Head of account as given in the original sanction letter	<b>Major Head –</b> <table border="1"> <tr> <th>Sanctioned Heads</th> <th>Funds allotted (Rs.)</th> </tr> <tr> <td>Staff</td> <td>4,87,000/-</td> </tr> <tr> <td>Equipment (including spares thereof)</td> <td>Nil</td> </tr> <tr> <td>Operation and Maintenance of equipment</td> <td>1,00,000/-</td> </tr> <tr> <td>Expendables</td> <td>1,80,000/-</td> </tr> <tr> <td>Travel</td> <td>50,000/-</td> </tr> <tr> <td>Contingencies</td> <td>50,000/-</td> </tr> <tr> <td>Visiting faculties</td> <td>Nil</td> </tr> <tr> <td>Procured services</td> <td>1,00,000/-</td> </tr> <tr> <td>Institutional overheads</td> <td>34,000/-</td> </tr> <tr> <td>Column Total</td> <td>10,01,000/-</td> </tr> </table>	Sanctioned Heads	Funds allotted (Rs.)	Staff	4,87,000/-	Equipment (including spares thereof)	Nil	Operation and Maintenance of equipment	1,00,000/-	Expendables	1,80,000/-	Travel	50,000/-	Contingencies	50,000/-	Visiting faculties	Nil	Procured services	1,00,000/-	Institutional overheads	34,000/-	Column Total	10,01,000/-
Sanctioned Heads	Funds allotted (Rs.)																							
Staff	4,87,000/-																							
Equipment (including spares thereof)	Nil																							
Operation and Maintenance of equipment	1,00,000/-																							
Expendables	1,80,000/-																							
Travel	50,000/-																							
Contingencies	50,000/-																							
Visiting faculties	Nil																							
Procured services	1,00,000/-																							
Institutional overheads	34,000/-																							
Column Total	10,01,000/-																							
6.	Amount brought forward from the previous financial year quoting DRDO letter No. & date in which the authority to carry forward the said amount was given.	i. Amount: Rs 96,667/- ii. Letter No.: ERIP/ER/202103001/M/01/1785 iii. date: 10/05/2021																						
7.	Amount received during the financial year (Please give no. and date of DRDO sanction letter for the amount)	i. Amount: Rs 9,06,965/- ii. Letter No.: UTR No. 365790749 dt 26.7.24 iii. date: 08.8.24 (email)																						
8.	Amount of interest accrued, if any, from the grants	Rs. 4,037/-																						
9.	Total amount that was available for expenditure (excluding commitments) during the financial year (SL. No 6 +7+8)	Rs. 10,07,669/-																						
10.	Actual expenditure (excluding commitments) incurred during the financial year (up to 2024.)	Rs. 7,88,164/-																						
11.	Balance amount available at the end of the financial year.	Rs. 2,19,505/-																						
12.	Unspent balance refunded, if any (Please give details of Cheque No. etc.)	Rs. 2,19,505/- (refunded through Demand Draft No. <del>SBI-Demand draft No. 848643...</del> )																						
13.	Amount allowed to be carried forward to the next financial year	Not applicable																						

SKDas  
29.1.25





तेजपुर विश्वविद्यालय

(केंद्रीय विश्वविद्यालय)

नपाम, तेजपुर - 784028, असम, भारत

TEZPUR UNIVERSITY

(A Central University)

Napaam, Tezpur - 784028, Assam, India

(सर्वोत्तम विश्वविद्यालय के लिए कुलाध्यक्ष पुरस्कार, 2016, भारत के 100 श्रेष्ठ उच्च शिक्षण संस्थानों में पंचम स्थान और 'नाक' द्वारा 'ए+' ग्रेड प्राप्त विश्वविद्यालय)  
(Awardee of Visitor's Best University Award, 2016, 5<sup>th</sup> among India's Top 100 Universities, MHRD-NIRF-Ranking, 2016 and NAAC Accredited with "A+" Grade)

**AUDITED UTILIZATION CERTIFICATE**  
(From April 01, 2024 to December 16, 2024)

Certified that out of a sum of (i) **Rs. 9,06,965/- (Rupees Nine Lakh Six Thousand Nine Hundred Sixty-Five only)** received as grants-in-aid for 1.04.2024-16.12.2024, in favor of Registrar, Tezpur University vide email intimation of NEFT credit in r/o Grants-in-aid Project No. 1785, dated 8 August 2024, (ii) **Rs. 4,037/- (Rupees Four Thousand Thirty-Seven only)** accrued as interest during 1.04.2024-16.12.2024, and (iii) **Rs 96,667/- (Rupees Ninety-Six Thousand Six-Hundred Sixty-Seven only)** on account of unspent balance of the previous Financial Year (01-04-2023 to 31-03-2024), a sum of **Rs. 7,88,164/- (Rupees Seven Lakh Eighty-Eight Thousand One Hundred Sixty-Four only)** has been utilized for the purpose for which it was sanctioned and that the balance of **Rs 2,19,505/- (Rupees Two Lakh Nineteen Thousand Five Hundred Five only)** remaining unutilized at the end of 1.04.2024-16.12.2024 is returned through Demand Draft (No. SBT Demand draft No. 848643.....) in favor of CDA (R&D), New Delhi.

*SKda82* 29.1.25  
Principal Investigator

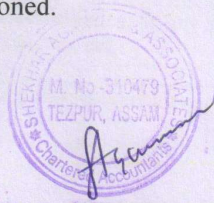
**Dr. Sajal Kumar Das**  
Assistant Professor  
Dept. of Chemical Sciences  
Tezpur University

*[Signature]*  
Accounts/Finance Officer  
Finance Officer  
Tezpur University

*[Signature]*  
Administrative Authority  
(with official seal)  
Registrar  
Tezpur University

2. Certified that I have satisfied myself that the conditions on which the grants-in-aid was sanctioned have been fulfilled/are being fulfilled and that I have exercised the following checks to see that the money was actually utilized for the purpose for which it was sanctioned.

For Shekhar Agarwal & Associates  
Chartered Accountants



Signature of Audit Authority  
of Grantee Institution

Shekhar Agarwal  
Proprietor  
Membership No.-310479  
ICAI FRN 329706E

Date - 21/02/2025

UDIN-25310479BMJUP7738